Available online at www.sciencedirect.com
SCIENCE DIRECT®
International Journal of Mass Spectrometry 241 (2005) 243–260
International Journal of Mass Spectrometry
www.elsevier.com/locate/ijms

Ammonia activation by iron: state-specific reactions of $Fe^+(^6D, ^4F)$ with ND_3 and the reaction of $FeNH^+$ with D_2

Rohana Liyanage[1], P.B. Armentrout*

Department of Chemistry, University of Utah, Salt Lake City, UT 84112, USA

Received 18 November 2004; accepted 2 December 2004
Available online 15 January 2005

In honor of Bill Hase's 60th birthday and in celebration of his many contributions to chemical dynamics.

Abstract

The kinetic energy dependence of the reactions of $Fe^+(^6D, ^4F)$ with ND_3, $FeNH^+$ with D_2, and $FeNH^+$ with Xe are studied in a guided ion beam tandem mass spectrometer over the energy range of 0–10 eV. Only two products, both formed in endothermic processes, are observed in the former system, $FeND_2^+$ and FeD^+. By using both dc discharge/flow tube and surface ionization sources, state-specific reaction cross sections for these products are obtained. In the reaction of $FeNH^+$ with D_2, four ionic products, Fe^+, $FeNHD^+$, $FeND_2^+$, and FeD^+, are observed. The latter three products are formed in endothermic reactions, whereas exothermic formation of $Fe^+ + NHD_2$ is shown to occur via a reaction barrier of 0.27 ± 0.05 eV. Analyses of the various endothermic reactions are used to obtain bond energies for $Fe^+{-}NH_2$ of 2.88 ± 0.12 eV and for $Fe^+{-}NH$ of 2.76 ± 0.09 eV. Combining these various results permits a fairly complete experimental evaluation of the potential energy surface for ammonia activation by Fe^+. The experimental information obtained is compared to calculated energetics and potential energy surfaces obtained using density functional theory (B3LYP/6-311++G(3df,3p)//B3LYP/6-311+G* and CCSD(T)/6-311++G(3df,3p)//B3LYP/6-311+G*) as well as previous experimental and theoretical results in the literature. Implications for the bond energy of $FeOH^+$ are also discussed.

Keywords: Ammonia; Bond energies; Guided ion beam; Iron; Thermochemistry; State-specific chemistry

1. Introduction

The interaction of ammonia with iron is important in understanding the catalytic synthesis of ammonia from N_2 and H_2, the Haber process, which utilizes an iron oxide catalyst with small amounts of Al_2O_3 and K_2O and sometimes other oxides added as promoters [1]. Ammonia is known to adsorb to iron surfaces nondissociatively at low temperatures, whereas at higher energies, stepwise dissociation occurs yielding a stable adsorbed NH intermediate, clearly a key intermediate in the production of NH_3 from N_2 and H_2. Energetics for the various intermediates, H, N, NH, NH_2, and NH_3, adsorbed to iron surfaces have been estimated [1], and recently we have examined the energetics of adsorbing these species to iron cluster cations [2,3]. This thermochemistry, some of the first experimental data for molecular fragments bound to metal surfaces of any size, is needed to fully understand such catalytic processes.

Because of the complexity of the electronic states of metal clusters, detailed studies (both experimental and theoretical) of the potential energy surfaces for a reaction like ammonia activation are difficult. However, such studies are tractable for the atomic iron system, which should provide a foundation for a better understanding of the interactions of ammonia with more complex iron species. In particular, the ability to experimentally study the state-specific chemistry of $Fe^+(^6D, ^4F)$ with ND_3 and the reverse reaction of $FeNH^+$ with D_2 should yield valuable insight into ammonia activation and production.

In addition to its relevance to our recent cluster studies, the present investigation also augments previous systematic

* Corresponding author. Tel.: +1 8015817885; fax: +1 8015818433.
E-mail address: armentrout@chem.utah.edu (P.B. Armentrout).
[1] Present address: Department of Chemistry and Biochemistry, University of Arkansas, USA.

1387-3806/$ – see front matter © 2004 Elsevier B.V. All rights reserved.
doi:10.1016/j.ijms.2004.12.006

studies of reactions of atomic transition metals with H_2, CH_4, NH_3, and H_2O [4–7]. Although experimental studies of the reactions of ammonia with many of the first row transition metal ions, Sc^+, Ti^+ [8], V^+ [9], Co^+, Ni^+, and Cu^+ [10], have been completed (and examined theoretically [11–13]), such studies are not available for Fe^+, even though state-specific studies of its reactions with H_2 [14], CH_4 [15,16], and D_2O [17] have been performed, as well as related studies of the "reverse" reactions of $FeCH_2^+ + H_2$ [16], $FeO^+ + H_2$ [17,18], and $FeS^+ + H_2$ [19]. State-specific studies of the $Fe^+ + NH_3$ system would be particularly valuable as Chiodo et al. have theoretically compared the potential energy surfaces for reaction of Fe^+ with CH_4, NH_3, and H_2O [20]. In the present study, we extend our work of understanding first row transition metal reactivity towards ammonia by studying the state-specific reactivity of Fe^+ in both its ground ^6D state and first excited ^4F state. To further elucidate the potential energy surface of the $FeNH_3^+$ system, we also study the reaction of $FeNH^+$ with D_2 as well as the collision-induced dissociation of the $FeNH^+$ molecule. The former results can be compared with previous ion cyclotron resonance (ICR) studies of this reaction at thermal energies [21]. In combination with theoretical work, the present study provides a complete theoretical and experimental investigation of the bond energies and the reaction potential energy surface, which can be compared to literature thermochemistry values [20–24].

2. Experimental and computational section

2.1. Experimental methods

Cross sections for reactions of interest are measured using a guided ion beam tandem mass spectrometer that has been described in detail elsewhere [25,26]. Fe^+ ions are produced in both a surface ionization (SI) source and in a direct current (dc) discharge/flow tube (DC/FT) source. In the DC/FT source, Fe^+ is made using a dc discharge source consisting of an iron cathode held at high negative voltage (1.5–3 kV) over which a flow of approximately 90% He and 10% Ar passes. Ar^+ ions created in the discharge are accelerated toward the iron cathode, sputtering off ionic and neutral metal atoms. The high-pressure environment in the DC/FT source creates Fe^+ ions primarily in their ^6D ground state, as determined in previous studies [16,17]. There, we characterized this beam as containing about 99.2 ± 0.2 and $97 \pm 1\%$ ^6D and 0.8 ± 0.02 and $2.8 \pm 1\%$ ^4F states, with variations depending on the exact source conditions, which are unfortunately not systematic as they apparently involve the concentrations of minor contaminants in the reactant and flow gases. The SI source is used to produce a beam containing a known distribution of excited state Fe^+ ions. In this source, $Fe(CO)_5$ is passed through a water-cooled inlet line into an evacuated source chamber and over a rhenium filament that is resistively heated to 2000 ± 100 K, as measured by optical pyrometry. Dissociation of the $Fe(CO)_5$ and ionization of the resultant iron atoms occurs on the filament. If the ions reach equilibrium at the filament temperature, this method should produce a beam with a Maxwell–Boltzmann distribution of states. The validity of this assumption has been discussed previously [27] and verified for Co^+ by van Koppen et al. [28]. At the filament temperature used, 2000 ± 100 K, Fe^+ is produced in a distribution containing $82.1 \pm 1.0\%$ ^6D, $17.7 \pm 1.0\%$ ^4F, and $<0.2 \pm 0.1\%$ ^4D electronic states, which have energies of 0.052, 0.300, and 1.032 eV, respectively, for a statistical average of all spin-orbit levels [29].

To produce $FeNH^+$, we first form FeO^+ by reaction of Fe^+ with N_2O introduced upstream in the flow tube of the DC/FT source. Then FeO^+ reacts with NH_3 introduced downstream in the flow tube to form $FeNH^+$ in an exothermic process [22]. The flow conditions used in this ion source provide in excess of 10^4 collisions between an ion and the buffer gas, which is assumed to thermalize the ions rotationally and vibrationally. During our analysis of the data for reactions of $FeNH^+$, we assume that the ions produced in this source are in their electronic ground state and that the internal energy of the $FeNH^+$ species is well described by a Maxwell–Boltzmann distribution of ro-vibrational states at 300 K. Previous work from this laboratory has shown that these assumptions are generally valid [30–35].

Ions produced in the sources are extracted, accelerated, and focused into a magnetic sector momentum analyzer for mass analysis. Mass selected ions are decelerated to a desired kinetic energy and focused into an octopole ion guide, which traps the ions in the radial direction [36]. The octopole passes through a static gas cell containing the reactant neutral gas, ND_3, D_2, or Xe, at relatively low pressures ($(5–30) \times 10^{-8}$ bar). Product ions and remaining reactant ions drift to the end of the octopole, where they are focused into a quadrupole mass filter for mass analysis and detected by a secondary electron scintillation detector using standard pulse counting techniques. Ion intensities are converted into absolute cross sections as described previously [25]. Absolute uncertainties in cross section magnitudes are estimated to be ±20%, and are largely the result of uncertainties in the pressure measurement and the length of the interaction region. Relative uncertainties in the cross sections are approximately ±5%.

Ion kinetic energies in the laboratory frame of reference, E_{lab}, are converted to energies in the center-of-mass frame, E_{cm}, using the formula $E_{cm} = E_{lab}m/(m + M)$, where M and m are the masses of the ionic and neutral reactants, respectively. All energies reported below are in the center-of-mass frame unless otherwise specified. The absolute zero and distribution of the ion kinetic energies are determined using the octopole ion guide as a retarding potential analyzer, as previously described [25]. The distribution of the ion kinetic energies is nearly Gaussian, with a FWHM typically between 0.5 and 0.7 eV (lab) for these experiments. The uncertainty in the absolute energy scale is ±0.05 eV (lab).

Pressure dependent studies were performed on all cross sections to determine the presence and magnitude of any

effects resulting from multiple collisions that may influence the shape of the reaction cross sections. Data free from pressure effects is obtained by extrapolating to zero reactant pressure, as described previously [37]. Thus, results reported below result from single bimolecular collisions exclusively.

2.2. Computational procedures

Although the potential energy surfaces for the reaction of Fe^+ with NH_3 have been studied theoretically before [20], these studies focused on the dehydrogenation reaction. In order to examine the alternate reaction channels observed here, calculations on all possible products and the potential energy surfaces involved were conducted using the Gaussian 98 suite of programs [38]. Geometry optimizations and frequency calculations utilized the B3LYP hybrid density functional method [39–41] with a 6-311+G* basis set, a level slightly higher than previous work [20]. Single point energies were calculated using both B3LYP and CCSD(T) methods with a 6-311++G(3df,3p) basis set, levels higher than previously performed [20]. In all cases, the thermochemistry reported here is corrected for zero point energy (ZPE) effects (with frequencies scaled by 0.989) [42]. For simplicity, these calculations will be referred to as B3LYP//B3LYP and CCSD(T)//B3LYP values. For many of the species, calculations of excited states were obtained by explicitly moving electrons into other orbitals to create states of alternate configuration and/or symmetry. Optimizations of the geometry were then carried out in the usual way. In all cases, frequency calculations verified the identity of the energy minima and first order saddle points.

The experimental splitting between the $^6D(4s^13d^6)$ ground state and $^4F(3d^7)$ excited state of Fe^+ is 0.248 eV, calculated as the average difference between properly weighted spin-orbit components of the ^6D (0.052 eV above the $^6D_{9/2}$ ground level) and ^4F (0.300 eV above the $^6D_{9/2}$ ground level) terms [29]. The calculated splitting is inverted at the B3LYP level, 0.218 eV using the 6-311+G* basis and 0.212 eV using the 6-311++G(3df,3p) basis set, whereas CCSD(T)/6-311++G(3df,3p) calculations find the right order and an excitation energy for the ^4F state of 0.502 eV. These results can be compared to the ^4F excitation energies calculated in the literature as −0.45 eV (B3LYP/DZVP), −0.18 eV (B3LYP/TZVP+G(3df,2p)), 0.54 (B3LYP/$DZVP_{opt}$, where $DZVP_{opt}$ indicates an Fe basis set optimized to yield the correct splitting for the atomic states) [20], and 0.23 eV (CCSD(T)/TZVP+G(3df,2p)) [43]. Because our calculations do not explicitly include spin-orbit interactions, all calculations involving an asymptote including Fe^+ are referenced to the average energy of the spin-orbit components of the ^6D term at 0.052 eV. To properly compare to experimental values, which refer to the energy of the $^6D_{9/2}$ ground state at 0.0 eV, the calculated values must be corrected for this asymptotic energy.

2.3. Threshold analysis and thermochemistry

Threshold regions of the reaction cross sections are modeled using Eq. (1)

$$\sigma(E) = \sigma_0 \sum g_i (E + E_{el} + E_i - E_0)^n / E \quad (1)$$

where σ_0 is an energy dependent scaling factor, E the relative translational energy of the reactants, E_0 the energy threshold for reaction of the ground electronic and ro-vibrational state, E_{el} the electronic energy of the reactant ion, and n is an adjustable parameter. The summation is over the ro-vibrational states of the reactants, i, where E_i is the excitation energy of each state and g_i is the population of those states ($\sum g_i = 1$). In the $Fe^+ + ND_3$ system, strong competition between product channels is evident from the energy dependence of the cross sections, such that these were analyzed using a statistical model for competition detailed elsewhere [44]. The assumption that products formed at threshold have an internal temperature of 0 K has been described and tested in detail previously [31,45]. Treating all forms of energy in the reactants (vibrational, rotational, and translational) as capable of coupling to the dissociation coordinate has been shown to lead to reasonable thermochemistry. The threshold energies for dissociation reactions, as determined by analysis with Eq. (1), are converted to bond dissociation energies (BDEs) by assuming that E_0 represents the energy difference between reactants and products. This assumption requires that there are no reverse activation barriers in excess of the endothermicity of dissociation, which is generally true for ion-molecule reactions because of the long-range ion-induced dipole and higher order interactions [46], although exceptions are found in the present system and carefully characterized. Because all sources of reactant energy are included in the threshold analysis, the BDEs determined correspond to the thermodynamic values at 0 K.

3. Results

3.1. $Fe^+ + ND_3$

Two ionic products are formed according to reactions 2 and 3

$$Fe^+ + ND_3 \rightarrow FeND_2^+ + D \quad (2)$$

$$\rightarrow FeD^+ + ND_2 \quad (3)$$

The cross sections for reactions 2 and 3 obtained from the DC/FT and SI sources are shown in Fig. 1. $FeND_3^+$ is also observed at low energies, but pressure dependent studies show that this species is formed by collisional stabilization. Extrapolation of these data to single collision conditions yields no residual cross section for adduct formation. Despite a careful search for $FeND^+$ and FeN^+ product ions, no evidence for their formation is observed, suggesting they have cross sections below $\sim 10^{-19}$ cm^2. The $FeND_2^+$ (SI) and $FeND_2^+$

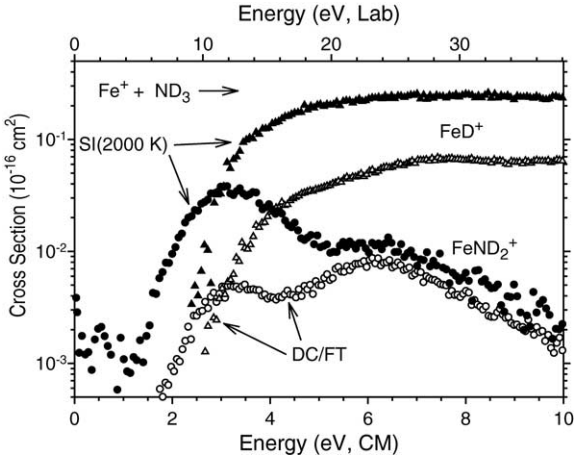

Fig. 1. Variation of product cross sections for reaction of ND_3 with Fe^+ produced in the surface ionization (SI, closed symbols) and dc discharge/flow tube (DC/FT, open symbols) sources to form $FeD^+ + ND_2$ (triangles) and $FeND_2^+ + D$ (circles) as a function of kinetic energy in the center-of-mass frame (lower *x*-axis) and laboratory frame (upper *x*-axis).

(DC/FT) cross sections exhibit two cross section features. One starts between 1 and 1.5 eV (at lower energies, the data shown corresponds to the noise level for these experiments) and peaks near the onset of reaction 3 indicating competition between the two reactions. The low energy feature in the $FeND_2^+$ (DC/FT) data has a magnitude about a factor of 10 smaller than that in the $FeND_2^+$ (SI) data. The high-energy feature in the $FeND_2^+$ cross section is most obvious in the DC/FT data, but is clearly present in the SI data as well. The absolute magnitudes of the high-energy features are comparable for Fe^+ produced in both sources. At higher energies, formation of FeD^+ dominates the reactivity as is typical for reactions of transition metal ions with CH_4 [5–7], NH_3 [8–10], and H_2O [17]. The relative magnitudes of the two high-energy features in the $FeND_2^+$ cross sections indicate that this feature must result from the reaction of the ^6D state (97–99% of the DC/FT beam and 82% of the SI beam). Likewise, the relative magnitudes of the two low energies features are consistent with the increased ^4F state population in the SI generated beam ($\sim 18 \pm 1\%$) compared to the population of this state generated in the DC/FT source (1–4%). Indeed, the factor of 10 ratio between these cross section features in the present system indicates that the DC/FT source in this study yields $1.8 \pm 0.2\%$ ^4F state, consistent with the previous characterizations. Considering that the conditions of the DC/FT source (discharge voltage, precise distribution of the flow gases, presence of contaminants) can all affect the detailed distribution of states, the agreement between studies taken over a decade apart is quite good. Thus, between 1 and 4 eV, the $FeND_2^+$ cross section is dominated by the ^4F state, whereas above 5 eV, the cross section is dominated by the ground ^6D state in both the SI and DC/FT data.

Although the changes observed for the FeD^+ data channel between SI and DC/FT data sets are not as striking as those observed for the $FeND_2^+$ data channel, the FeD^+ cross sections clearly differ, Fig. 1. The FeD^+ (SI) cross section rises more rapidly with increasing energy and has a lower apparent threshold than does Fe^+(DC/FT). Thus the threshold region of the FeD^+ (SI) cross section is dominated by reaction of the ^4F state ions.

3.2. State-specific cross sections for $Fe^+(^6D)$ and $Fe^+(^4F) + ND_3$

The SI and DC/FT cross sections displayed in Fig. 1 can be used to derive state-specific cross sections for reaction of $Fe^+(^6D)$ and $Fe^+(^4F)$ with ND_3. As explained above, from a comparison of the lower energy features in the $FeND_2^+$ cross sections for the DC/FT and SI data, we estimate the ^4F state population in the DC/FT source as $1.8 \pm 0.2\%$. Assuming the contributions of higher lying excited states to the reaction are negligible, the remaining 98.2% of the ions are in the ^6D state. This result is comparable to the 99.2 ± 0.2 and $97 \pm 1\%$ amount of ^6D state determined in previous studies [16,17]. State-specific $FeND_2^+$ and FeD^+ cross sections are obtained by solving the simultaneous equations (4) and (5)

$$\sigma^{SI} = 0.18\sigma(^4F) + 0.82\sigma(^6D) \quad (4)$$

$$\sigma^{DC/FT} = 0.02\sigma(^4F) + 0.98\sigma(^6D) \quad (5)$$

σ^{SI} and $\sigma^{DC/FT}$ are the total cross section for a given product, $FeND_2^+$ or FeD^+, generated under the SI or DC/FT source conditions, respectively. State-specific reaction cross sections obtained for $Fe^+(^6D)$ and $Fe^+(^4F)$ states are shown in Fig. 2. On the basis of these state-specific cross sections, it is clear that the ^4F state is about six (FeD^+) and 20 ($FeND_2^+$) times more reactive than the ground ^6D state in the reaction with ND_3. Similar reactivity differences for these states were observed in reactions with H_2O and CH_4, with differences of about 5–25 (depending on the product) [15,17].

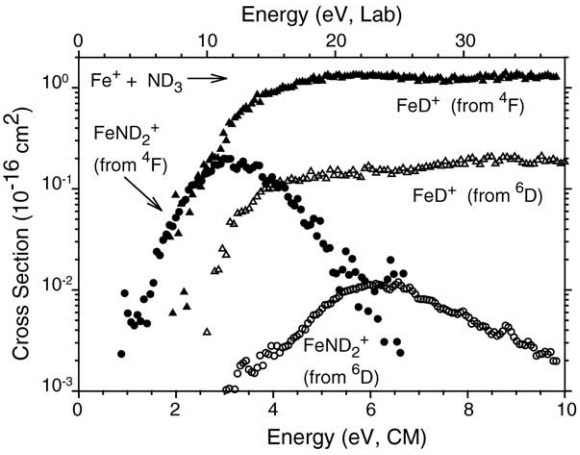

Fig. 2. State-specific cross sections for the reaction of ammonia with Fe^+ as a function of kinetic energy in the laboratory frame (upper *x*-axis) and center-of-mass frame (lower *x*-axis). Solid symbols show product cross sections for reaction of $Fe^+(^4F)$ and open symbols show product cross sections for reaction of $Fe^+(^6D)$. Triangles show the $FeD^+ + ND_2$ product channel and circles show the $FeND_2^+ + D$ channel.

Table 1
Summary of parameters used in Eq. (1) for fitting cross sections

Product	σ_0	n	E_0 (eV)
$Fe^+(^6D) + ND_3 \rightarrow FeD^+ + ND_2$	0.02 ± 0.02	1.9 ± 0.2	3.0 ± 0.3
	0.01 ± 0.01	2.3 ± 0.2	2.8 ± 0.3[a]
$Fe^+(^4F) + ND_3 \rightarrow FeD^+ + ND_2$	1.9 ± 0.3	1.2 ± 0.1	2.78 ± 0.05
	0.6 ± 0.3	1.0 ± 0.1	2.57 ± 0.10[a]
$Fe^+(^6D) + ND_3 \rightarrow FeND_2^+ + D$	0.002 ± 0.001	1.9 ± 0.2	2.1 ± 0.3[b]
$Fe^+(^4F) + ND_3 \rightarrow FeND_2^+ + D$	0.3 ± 0.1	1.6 ± 0.2	1.84 ± 0.15[b]
$FeNH^+ + Xe \rightarrow Fe^+ + NH$	1.6 ± 0.3	1.3 ± 0.2	3.04 ± 0.15
$FeNH^+ + D_2 \rightarrow Fe^+ + NHD_2$	0.4 ± 0.1	2.1 ± 0.1	0.27 ± 0.05
$FeNH^+ + D_2 \rightarrow Fe^+ + NH + D_2$	1.5 ± 0.6	1.2 ± 0.4	3.1 ± 0.3
$FeNH^+ + D_2 \rightarrow FeNHD^+ + D$	0.5 ± 0.1	2.6 ± 0.4	0.38 ± 0.05
$FeNH^+ + D_2 \rightarrow FeND_2^+ + H$	0.1 ± 0.1	2.6 ± 0.4	0.35 ± 0.10
$FeNH^+ + D_2 \rightarrow FeD^+ + NHD$	0.2 ± 0.1	1.1 ± 0.1	1.2 ± 0.2

[a] Competition with reaction 2 is considered during the threshold modeling.
[b] Values are the same whether competition with reaction 3 is considered or not.

The rationale for this strong state dependence is discussed below.

These state-specific cross sections are analyzed for thresholds using Eq. (1) and provide the parameters given in Table 1. Given the E_{el} values of 0.052 and 0.300 eV for $Fe^+(^6D)$ and $Fe^+(^4F)$, respectively [29], the sextet and quartet states yield 0 K thresholds of 3.0 ± 0.3 and 2.78 ± 0.05 eV, respectively, for reaction 3 if competition with reaction 2 is not considered. As discussed below, formation of $FeD^+ + ND_2$ and $FeND_2^+ + D$ must evolve from the same D–Fe^+–ND_2 intermediate and therefore compete with one another. Such competition can inhibit observation of the product with the higher threshold (here, FeD^+), leading to a competitive shift to higher energies. Statistical methods for describing competition have been devised [44] and when these are used to simultaneously analyze the cross sections for reactions 2 and 3, the E_0 thresholds for reaction 3 with the ^6D and ^4F states change to 2.8 ± 0.3 and 2.57 ± 0.10 eV, respectively, Table 1. As these threshold values are within experimental error of one another, they help confirm the state assignments of the cross section, especially as the next possible state (^4D) is 1.032 eV higher in energy [29]. Similarly for reaction 2, the thresholds (both with and without competition included) are 2.1 ± 0.3 and 1.84 ± 0.15 eV for the ^6D and ^4F cross sections, respectively, again within experimental error of one another.

3.3. CID of $FeNH^+$

Cross sections for collision-induced dissociation (CID) of $FeNH^+$ with Xe are shown in Fig. 3. $FeNH^+$ dissociates by cleaving the Fe–N bond to produce Fe^+ and NH in reaction 6

$$FeNH^+ + Xe \rightarrow Fe^+ + NH + Xe \quad (6)$$

however, observation of a $FeN^+ + H$ product channel would be difficult in our instrument because of mass overlap with the much more intense reactant ion signal. The Fe^+ cross section rises slowly from a threshold near 3 eV and starts to level off above 6 eV. Analysis of the Fe^+ cross section using Eq. (1) yields a threshold of 3.04 ± 0.15 eV. This threshold could be larger than the thermodynamic threshold as we have observed that CID of strong covalently bound species often gives a high threshold because the efficiency of collisional energy transfer may be limited in such systems [47,48]. Hence the threshold obtained this way should be a good upper limit to the Fe^+–NH BDE.

3.4. $FeNH^+ + D_2$

$FeNH^+$ reacts with D_2 to yield four ionic products corresponding to reactions 7–11

$$FeNH^+ + D_2 \rightarrow Fe^+ + NHD_2 \quad (7)$$

$$\rightarrow Fe^+ + NH + D_2 \quad (8)$$

$$\rightarrow FeNHD^+ + D \quad (9)$$

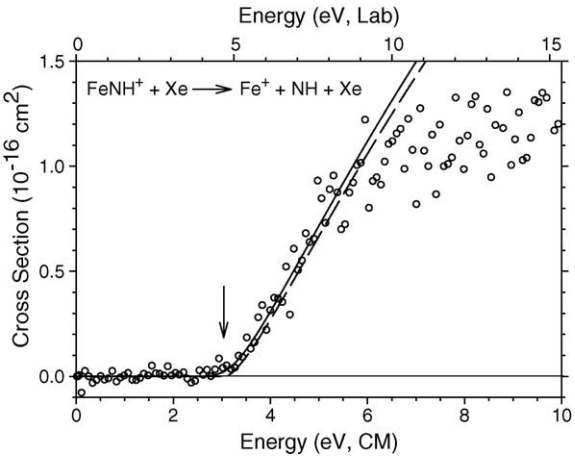

Fig. 3. Cross sections for collision-induced dissociation of $FeNH^+$ with Xe as a function of kinetic energy in the laboratory frame (upper *x*-axis) and center-of-mass frame (lower *x*-axis). The best fit to the Fe^+ data using Eq. (1) with parameters in Table 1 is shown as a dashed line. The solid line shows this model convoluted over the kinetic and internal energy distributions of the neutral reactant and ion. The arrow shows the threshold energy derived from this analysis, 3.04 eV.

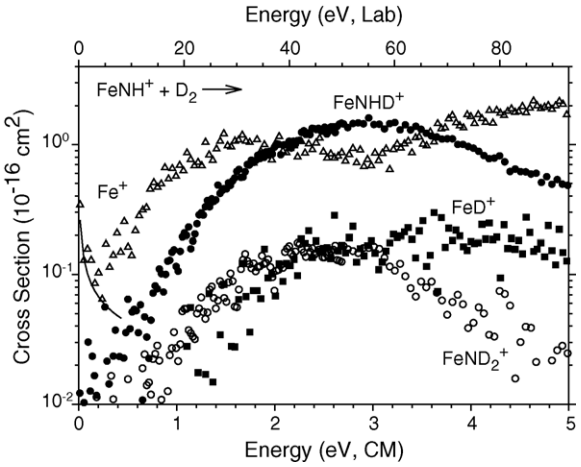

Fig. 4. Variation of product cross sections for reaction of $FeNH^+$ with D_2 to form Fe^+ (open triangles), $FeNHD^+$ (solid circles), $FeND_2{}^+$ (open circles), and FeD^+ (solid squares) as a function of kinetic energy in the center-of-mass frame (lower *x*-axis) and laboratory frame (upper *x*-axis). The line shows the LGS collision cross section times 0.002.

$$\rightarrow \mathrm{FeND_2}^+ + \mathrm{H} \quad (10)$$

$$\rightarrow \mathrm{FeD}^+ + \mathrm{NHD} \quad (11)$$

as shown in Fig. 4. The Fe^+ product shows two features in its cross section that can be attributed to reactions 7 and 8. Reaction 7 is lower in energy as it forms the stable NHD_2 molecule, whereas reaction 8 corresponds to simple CID of the reactant $FeNH^+$ molecule to $Fe^+ + NH$. At the lowest energies (<0.2 eV), there is also evidence for a small amount of exothermic reactivity. In this region, the cross section declines as $E^{-1/2}$, consistent with the energy dependence of the collision cross section predicted by the Langevin–Gioumousis–Stevenson (LGS) model [49], but having a magnitude 0.0015 ± 0.0007 times this prediction. Threshold analysis of the first endothermic feature (after subtracting $0.0015 \pm 0.0007\sigma_{LGS}$) gives an average threshold value of 0.27 ± 0.05 (Table 1). As noted above, we presume that the reactants have a Maxwell–Boltzmann distribution of internal energies at 300 K, and if so, then 0.3% of the reactants have energies exceeding 0.27 eV, more than enough to explain the very small exothermic feature observed here presuming that these ions react with an energy dependence like σ_{LGS} (i.e., the *n* value in Eq. (1) changes to 0.5 for these ions). After subtracting a model for this lower energy feature from the total cross section, the second feature can be analyzed and gives a threshold value of 3.1 ± 0.3 eV, consistent with the CID threshold obtained in reaction 6 with Xe above.

It is clear that the cross section for the Fe^+ product starts decreasing around 1.5 eV, and this decrease correlates with an increase in the $FeNHD^+$ product cross section. This is an indication of competition between these two reaction pathways. The chemically analogous product, $FeND_2{}^+$, is also observed but is formed much less efficiently than $FeNHD^+$. Data analyses of the cross sections for reactions 9 and 10 find thresholds of 0.38 ± 0.05 and 0.35 ± 0.10 eV, respectively, Table 1. The small differences can be attributed to the zero point difference for the two products. Using the vibrational frequencies calculated here, this zero point energy difference is calculated to be 0.08 ± 0.01 eV in favor the $FeND_2{}^+$ product, consistent with the 0.03 ± 0.11 eV difference measured. The least efficient process is reaction 11, which must be competing with reaction 9. The threshold for the FeD^+ product ion is measured as 1.2 ± 0.2 eV, Table 1. It seems likely that FeH^+ and $FeND^+$ would also be formed, but neither were observed despite looking for them. The efficiency for formation of FeH^+ compared to FeD^+ production should probably mimic the relative cross sections for reactions 9 versus 10. Consequently, the anticipated maximum magnitude of the FeH^+ cross section is less than 0.02×10^{-16} cm^2, close to the noise limit of these experiments. Formation of $FeND^+$ is also expected to be inefficient for reasons discussed below, and in addition, this product would be difficult to observe as it lies in between the very intense reactant ion beam and the $FeNHD^+$ product ion. Because of the proximity to these other ions, we conservatively estimate that the cross section for $FeND^+$ lies below 10^{-17} cm^2.

4. Thermochemical and theoretical results

Bond energies for $D_0(Fe^+–H)$, $D_0(Fe^+–NH)$, and $D_0(Fe^+–NH_2)$ can be obtained from thresholds for reactions 2, 3, 6–11 with the help of the thermochemistry listed in Table 2 and zero point energy corrections taken from the calculations performed here. Table 3 lists the final bond energies determined here along with literature values for comparison. Calculated vibrational and rotational frequencies are listed in Table 4. The following sections describe the experimental thermochemistry derived in this fashion for each of the ionic products along with our theoretical characterization of these species. Table 5 summarizes the calculated energies and zero point energies for the various species discussed below. Table 6 and Fig. 5 characterize the geometries of these species.

Table 2
Bond dissociation energies for NH_n and ND_n species at 0 K[a]

Bond	D_0 (eV)	Bond	D_0 (eV)
H–H	4.4781 ± 0.0001	D–D	4.5563 ± 0.0001
N–H	3.419 ± 0.010	N–D	3.474 ± 0.010
HN–H	3.949 ± 0.015	DN–D	4.033 ± 0.015
DN–H	3.963 ± 0.015	HN–D	4.018 ± 0.015
H_2N–H	4.632 ± 0.011	D_2N–D	4.752 ± 0.011
HN–H_2	4.103 ± 0.011	DN–D_2	4.229 ± 0.011

[a] Heats of formation for most species are taken from Ref. [53]. Those for NH and NH_2 are from [55]. Values for deuterated species are adjusted from the perprotio species using molecular constants given in Ref. [53], except for the NHD species which utilizes values calculated here at the B3LYP/6-311+G* level.

Table 3
Bond dissociation energies (eV) of Fe^+—NH_x (x = 1–3) and Fe^+—H at 0 K

	Experiment		Theory	
	This work	Literature	This work[a]	Literature
$D(Fe^+—H)$	2.15 ± 0.10	2.12 ± 0.06[b]	2.10 (2.02)	2.04[c], 2.26[d] 2.13 (2.27)[e]
$D(Fe^+—NH)$	2.76 ± 0.09	>1.78, <3.51[f] 2.78 ± 0.09 (2.99 ± 0.09)[g] 2.65 ± 0.22[h]	2.40 (2.43)	2.51[d], 2.51[g]
$D(Fe^+—NH_2)$	2.88 ± 0.12	>2.38, <3.43[f] 3.20 ± 0.10[i]	2.94 (2.89)	3.23[d]
$D(Fe^+—NH_3)$		1.90 ± 0.12[j]	1.76 (1.85)	2.02[d], 1.98[k]

[a] CCSD(T)/6-311++G(3df,3p)//B3LYP/6-311+G* (B3LYP/6-311++G(3df,3p)//B3LYP/6-311+G* relative to the Fe^+(^{4}F) asymptote) values from this work including zero point energy corrections.
[b] Refs. [45,50].
[c] Ref. [51].
[d] Ref. [20].
[e] Ref. [52].
[f] Ref. [22].
[g] Ref. [21] as revised in the text. Originally cited value in parentheses.
[h] Photodissociation value from Refs. [22,24].
[i] Ref. [45].
[j] Ref. [57].
[k] Ref. [56].

4.1. Fe^+–H

The most reliable value for $D_0(Fe^+—H)$, 2.12 ± 0.06 eV, has been determined previously from the reactions of Fe^+ with H_2 and D_2 [45,50]. Using this BDE, a ZPE difference for FeH^+ versus FeD^+ of 0.030 eV [50], and the relationship $E_0(3) = D_0(ND_2—D) - D_0(Fe^+—D)$, the predicted 0 K threshold for the FeD^+ product in the ammonia reaction 3 is 2.60 ± 0.06 eV. When the thresholds are measured for this process without considering the competition with reaction 2, the values are higher than the predicted value, 2.78 ± 0.05 eV for the ^{4}F state and 3.0 ± 0.3 eV for the ^{6}D state, Table 1. When the competition with reaction 2 is included, we find a threshold of 2.57 ± 0.10 eV for the ^{4}F state and 2.8 ± 0.3 eV for the ^{6}D state, which agree well with the expected value.

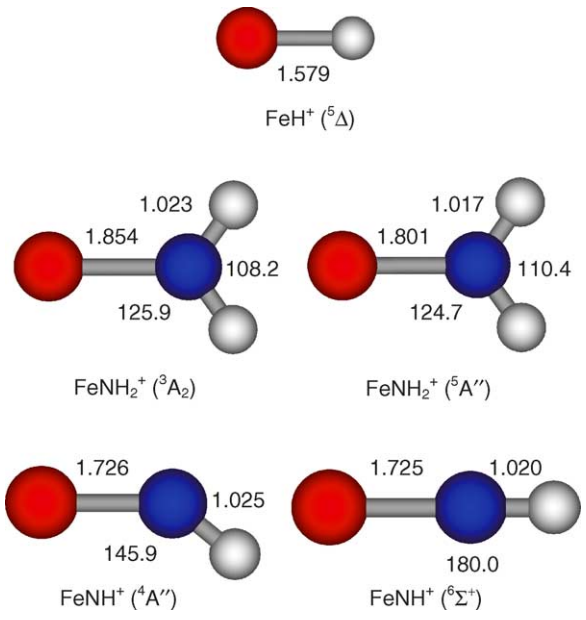

Fig. 5. Geometries for low energy states of FeH^+, $FeNH_2^+$, and $FeNH^+$ calculated at the B3LYP/6-311+G* level. Bond distances shown are in Å and angles are in °.

Previously, Schilling et al. [51] and Pettersson et al. [52] have characterized the low-lying states of FeH^+. Both studies find a $^5\Delta$ ground state with a valence electron configuration of $\sigma_b^2\delta^3\pi^2\sigma^1$, where σ_b is the bonding orbital, the δ and π orbitals are largely metal-based 3d orbitals, and the σ orbital is a nonbonding orbital. Schilling et al. find that the late metal ions have bonding orbitals with metal character of 74% 4s, 12% 4p, and 14% 3dσ, whereas results of Pettersson et al., in which the 3d–3d correlation energy is better handled, suggest more 3d character, 51% 4s, 13% 4p, and 36% 3dσ. Schilling et al. also found low-lying $^5\Pi(\sigma_b^2\delta^2\pi^3\sigma^1)$ and $^5\Sigma^+(\sigma_b^2\delta^2\pi^2\sigma^2)$ states lying only 0.091 and 0.434 eV higher in energy. Schilling et al. find these states to have bond lengths (r_e) of 1.653, 1.641, and 1.663 Å, respectively, whereas Pettersson et al. find a ground state bond length of 1.603 Å (1.598 Å including relativistic effects). Pettersson et al. suggest that the difference in bond lengths between their work and that of Schilling et al. is a consequence of neglecting the correlation energy associated with the d orbitals in the latter work. In agreement with these results, our calculations find these three states with bond lengths of 1.579, 1.561, and 1.635 Å, more like those of Pettersson et al., and excitation energies of 0.0, 0.104 eV (0.162), and 0.479 eV (0.733), respectively, for the CCSD(T)//B3LYP (B3LYP//B3LYP) calculations, in agreement with Schilling et al.

The ground state bond energies calculated in each of these studies are 2.04 [51] and 2.13 eV (2.27 eV after approximate

Table 4
Rotational constants and vibrational frequencies calculated at the B3LYP/6-311+G* level[a]

Species	State	B (cm^{-1})	ω (cm^{-1})
H_2	$^1\Sigma_g^+$	60.78	4394
D_2	$^1\Sigma_g^+$	30.41	3108
NH	$^3\Sigma^-$	16.51 (2)	3259
ND	$^3\Sigma^-$	8.811 (2)	2379
NH_2	$^2B_1$	23.74, 12.73, 8.286	1567, 3340, 3434
ND_2	$^2B_1$	13.37, 6.372, 4.315	1152, 2413, 2527
NHD	$^2B_1$	20.11, 7.992, 5.719	1376, 2468, 3389
NH_3	$^1A_1$	10.02 (2), 6.214	1059, 1736 (2), 3475, 3604 (2)
ND_3	$^1A_1$	5.166 (2), 3.112	806, 1201 (2), 2483, 2657 (2)
FeH^+	$^5\Delta$	6.830 (2)	1875
	$^5\Pi$	6.988 (2)	1858
	$^5\Sigma$	6.371 (2)	1735
FeD^+	$^5\Delta$	3.478 (2)	1338
FeN^+	$^5\Delta$	0.520	569
	$^5\Phi$, $^5\Pi$	0.546	687
$FeNH^+$	$^6\Sigma^+$	0.432 (2)	325 (2), 723, 3535
	$^4A''$	58.96, 0.440, 0.436	317, 712, 3473
	$^4A'$	46.70, 0.440, 0.436	390, 709, 3458
	$^6A''$	343.6, 0.377, 0.376	130, 622, 3518
	$^2\Delta$	0.417 (2)	383 (2), 524, 3402
	$^2\Sigma$	0.438 (2)	395 (2), 504, 3444
	$^6A'$	25.77, 0.260, 0.258	258, 453, 3297
	$^4\Pi$	0.256 (2)	266, 540, 541, 3320
	$^4\Sigma^-$	0.245 (2)	280, 533, 550, 3322
$FeND^+$	$^6\Sigma$	0.378 (2)	248 (2), 702, 2593
$FeNH_2^+$	$^5A_1$	11.99, 0.378, 0.367	489, 644, 678, 1573, 3499, 3592
	$^5A''$	11.98, 0.380, 0.369	260, 653, 692, 1574, 3500, 3593
	$^5A_2$	11.99, 0.380, 0.369	−398, 651, 695, 1573, 3501, 3594
	$^3A_2$	12.18, 0.359, 0.348	499, 655, 686, 1626, 3437, 3533
	$^3B_1$	12.12, 0.345, 0.335	471, 526, 587, 1585, 3444, 3531
	$^3A_1$	12.14, 0.358, 0.348	480, 675, 746, 1625, 3430, 3510
	$^5B_1$	12.07, 0.273, 0.266	325, 511, 947, 1586, 3392, 3486
	$^3B_2$	11.87, 0.392, 0.379	685, 705, 775, 1604, 3486, 3581
	$^5B_2$	12.08, 0.259, 0.253	327, 514, 763, 1584, 3386, 3484
	$^5A_2$	12.15, 0.244, 0.239	308, 481, 711, 1578, 3387, 3483
	$^5A_1$	12.15, 0.244, 0.239	306, 476, 703, 1577, 3385, 3482
$FeND_2^+$	$^5A''$	6.00, 0.325, 0.308	202, 491, 649, 1177, 2530, 2650
$FeNHD^+$	$^5A''$	8.255, 0.351, 0.335	238, 540, 685, 1398, 2587, 3549
$FeNH_3^+$	$^4A_1$	6.314, 0.281 (2)	422, 697 (2), 1393, 1725 (2), 3439, 3525 (2)
	^6E	6.259, 0.248 (2)	346, 608 (2), 1369, 1710 (2), 3424, 3517 (2)
	^6A	6.277, 0.229 (2)	303, 567, 584, 1339, 1716, 1742, 3439, 3529, 3542
$FeND_3^+$	$^4A_1$	3.159, 0.233 (2)	395, 520 (2), 1059, 1248 (2), 2463, 2593 (2)
TS1	^4A	4.907, 0.370, 0.365	−691, 423, 625, 874, 897, 1615, 1672, 3462, 3552
	$^6A''$	4.915, 0.304, 0.301	−898, 453, 556, 772, 779, 1402, 1575, 3433, 3536
	^6A	5.057, 0.296, 0.293	−1168, 425, 571, 810, 988, 1414, 1589, 3427, 3530
$HFeNH_2^+$	$^4A''$	4.331, 0.386, 0.376	268, 434, 653, 725, 731, 1582, 1792, 3445, 3536
	$^6A'$	6.242, 0.355, 0.318	382, 424, 526, 650, 671, 1601, 1846, 3454, 3539
	$^4A'$	4.279, 0.385, 0.375	−510, 367, 492, 651, 756, 1573, 1753, 3451, 3483
	$^6A''$	9.586, 0.254, 0.248	176, 390, 532, 577, 661, 1600, 1910, 3423, 3508
TS2	^4A	3.062, 0.423, 0.383	−1288, 485, 565, 664, 760, 1128, 1435, 1974, 3391
	$^6A'$	3.664, 0.397, 0.358	−1850, 524, 604, 677, 813, 1044, 1616, 1735, 3494
	$^6A''$	3.723, 0.337, 0.309	−1796, 495, 531, 570, 890, 996, 1596, 1681, 3475
d^2-TS2	^4A	1.683, 0.414, 0.341	−939, 385, 522, 624, 701, 903, 1020, 1414, 3391
$(H_2)FeNH^+$	$^6A_1$	55.94, 0.342, 0.339	270, 272, 444, 481, 688, 720, 996, 3544, 3908
	$^4B_1$	56.90, 0.342, 0.340	87, 126, 232, 556, 664, 741, 862, 3529, 4021
	$^4B_2$	56.85, 0.343, 0.341	40, 45, 191, 567, 666, 751, 870, 3531, 4016
	$^6B_1$	56.44, 0.303, 0.301	110, 146, 325, 424, 607, 682, 929, 3526, 3966
	$^6B_2$	57.23, 0.302, 0.301	−104, 147, 258, 422, 621, 673, 814, 3531, 4063
	$^4A_2$	53.38, 0.338, 0.335	224, 254, 677, 734, 821, 829, 1339, 3563, 3605
	$^6A_2$	60.64, 0.197, 0.196	−25, 14, 42, 117, 218, 578, 592, 3306, 4380

[a] Degeneracies in parentheses.

corrections for relativistic effects, correlation, and basis set incompleteness) [52]. Chiodo et al. [20] calculate a value of 2.26 eV at the B3LYP/DZVP$_{opt}$ level. The present CCSD(T)//B3LYP result is 2.10 eV, which includes ZPE corrections and an adjustment for the spin-orbit level of Fe^+(^{6}D). All the theoretical values are in reasonable agreement with the experimental value. At the B3LYP//B3LYP level where the relative energies of the ^{6}D and ^{4}F states of Fe^+ are inverted, our calculations yield a bond energy of 2.02 eV if the calculation is referenced to the ^{4}F asymptote and corrected by the experimental excitation energy of 0.300 eV, whereas reference to the ^{6}D asymptote leads to a bond energy of 2.48 eV,

Table 5
Calculated energies and zero point energies (hartrees) for $FeNH_x^+$ species and fragments[a]

Species	State	ZPE(unsc)[b]	B3LYP/6-311+G*	B3LYP/6-311++G(3df,3p)	CCSD(T)/6-311++G(3df,3p)
Fe^+	^{6}D		−1263.355874	−1263.356816	−1262.289117
	^{4}F		−1263.363893	−1263.364594	−1262.270661
H	^{2}S		−0.502156	−0.502257	−0.499818
H_2	$^1\Sigma_g^+$	0.010010	−1.176632	−1.180028	−1.171050
N	^{4}S		−54.600723	−54.600723	−54.512703
NH	$^3\Sigma^-$	0.007426	−55.237638	−55.243286	−55.139406
NH_2	$^2B_1$	0.019002	−55.892955	−55.904654	−55.792298
NH_3	$^1A_1$	0.034662	−56.572824	−56.586798	−56.471426
FeH^+	$^5\Delta$	0.004272	−1263.953510	−1263.956212	−1262.872268
	$^5\Pi$	0.004234	−1263.947481	−1263.950250	−1262.868437
	$^5\Sigma$	0.003955	−1263.926658	−1263.929281	−1262.854656
FeN^+	$^3\Delta$	0.001297	−1318.042926	−1318.047612	−1316.741925
	$^5\Phi$, $^5\Pi$	0.001565	−1318.017771	−1318.022646	−1316.848584
$FeNH^+$	$^6\Sigma^+$	0.011184	−1318.704681	−1318.711900	−1317.520361
	$^4A''$	0.010258	−1318.699596	−1318.708190	−1317.517131
	$^4A'$	0.010380	−1318.699037	−1318.707800	−1317.517127
	$^6A''$	0.009727	−1318.684497	−1318.691807	
	$^2\Delta$	0.010691	−1318.679523	−1318.686154	−1317.468893
	$^2\Sigma^+$	0.010797	−1318.642434	−1318.651516	−1317.429175
	$^6A'$	0.009129	−1318.555938	−1318.563871	−1317.399682
	$^4\Pi$	0.010631	−1318.507201	−1318.513447	
	$^4\Sigma^-$	0.010675	−1318.436387	−1318.443079	
$FeNH_2^+$	$^5A_1$	0.023866	−1319.381170	−1319.391441	−1318.195998
	$^5A''$	0.023400	−1319.379429	−1319.389986	−1318.196034
	$^3A_2$	0.023735	−1319.350292	−1319.359089	−1318.145895
	$^3B_1$	0.023111	−1319.345458	−1319.354330	−1318.161766
	$^3A_1$	0.023845	−1319.339931	−1319.349245	−1318.152976
	$^5B_1$	0.023344	−1319.313771	−1319.322411	
	$^3B_2$	0.023504	−1319.308227	−1319.318984	
	$^5B_2$	0.022913	−1319.212726	−1319.221232	−1318.145036
	$^5A_2$	0.022666	−1319.208103	−1319.216457	
	$^5A_1$	0.022620	−1319.203575	−1319.212205	
$FeNH_3^+$	$^4A_1$	0.039066	−1320.024599	−1320.034809	−1318.831502
	^6E	0.038289	−1320.004666	−1320.014732	−1318.830372
	^6A	0.038184	−1319.989284	−1319.999529	
TS1	^4A	0.029895	−1319.937648	−1319.951147	−1318.752662
	$^6A''$	0.028494	−1319.900199	−1319.911583	−1318.707356
	^6A	0.029059	−1319.895426	−1319.906946	−1318.709768
$HFeNH_2^+$	$^4A''$	0.029993	−1319.944806	−1319.957407	−1318.750706
	$^6A'$	0.029831	−1319.941364	−1319.952497	−1318.748407
	$^4A'$	0.028536	−1319.941984	−1319.954325	
	$^6A''$	0.029109	−1319.925529	−1319.935830	
TS2	^4A	0.023700	−1319.863709	−1319.881471	−1318.680742
	$^6A'$	0.023937	−1319.862961	−1319.878931	−1318.678742
	$^6A''$	0.023360	−1319.841321	−1319.856631	
$(H_2)FeNH^+$	$^6A_1$	0.025791	−1319.904749	−1319.918476	−1318.716382
	$^4B_1$	0.024646	−1319.896083	−1319.910960	−1318.702571
	$^4B_2$	0.024324	−1319.894986		
	$^6B_1$	0.024409	−1319.881990	−1319.895834	
	$^6B_2$	0.023987	−1319.880548	−1319.894351	
	$^4A_2$	0.027445	−1319.860895		
	$^6A_2$	0.021066	−1319.727159	−1319.739050	

[a] Geometries of all species calculated at the B3LYP/6-311+G* level.
[b] Unscaled zero point energies.

Table 6
Theoretical geometries for H_2, NH_x ($x = 1$–3), FeH^+, and $FeNH_x^+$ ($x = 0$–3)[a]

Species	State	r(FeN)	r(FeH)	r(NH)	r(HH)	∠HFeN	∠FeNH	∠HNH	∠HFeNH
H_2	$^1\Sigma_g^+$				0.742				
NH	$^3\Sigma^-$			1.042					
NH_2	$^2B_1$			1.029 (2)				103.9	
NH_3	$^1A_1$			1.014 (3)				108.0 (3)	
FeH^+	$^5\Delta$		1.579						
	$^5\Pi$		1.561						
	$^5\Sigma$		1.635						
FeN^+	$^3\Delta$	1.701							
	$^5\Phi$,$^5\Pi$	1.660							
$FeNH^+$	$^6\Sigma^+$	1.725		1.020			180.0		
	$^4A''$	1.726		1.025			145.9		
	$^4A'$	1.731		1.026			141.1		
	$^6A''$	1.858		1.022			166.5		
	$^2\Delta$	1.756		1.030			180.0		
	$^2\Sigma^+$	1.711		1.028			180.0		
	$^6A'$	2.292		1.043			125.2		
	$^4\Pi$	2.269		1.038			180.0		
	$^4\Sigma^-$	2.323		1.038			180.0		
$FeNH_2^+$	$^5A_1$	1.806		1.017 (2)			124.8 (2)	110.4	180.0
	$^5A''$	1.801		1.017 (2)			124.7 (2)	110.4	176.8
	$^3A_2$	1.854		1.023 (2)			125.9 (2)	108.2	180.0
	$^3B_1$	1.893		1.023 (2)			125.7 (2)	108.6	180.0
	$^3A_1$	1.856		1.023 (2)			125.8 (2)	108.4	180.0
	$^5B_1$	2.142		1.027 (2)			125.9 (2)	108.2	180.0
	$^3B_2$	1.774		1.017 (2)			124.4 (2)	111.2	180.0
	$^5B_2$	2.201		1.028 (2)			125.9 (2)	108.1	180.0
	$^5A_2$	2.267		1.028 (2)			126.1 (2)	107.7	180.0
	$^5A_1$	2.270		1.028 (2)			126.2 (2)	107.7	180.0
$FeNH_3^+$	$^4A_1$	2.040		1.021 (3)			113.0 (3)	105.7 (3)	
	^6E	2.185		1.022 (3)			112.5 (3)	106.3 (3)	
	^6A	2.275		1.021 (3)			112.6 (3)	106.2 (3)	
TS1	^4A	1.802	1.601	1.020 (2), 1.760		61.9	121.4, 121.3	108.6	±71.9
	$^6A''$	1.992	1.698	1.023 (2), 1.794		57.5	125.0 (2)	109.3	±84.6
	^6A	2.020	1.715	1.023 (2), 1.741		54.8	125.0, 125.2	108.8	83.4, 83.8
$HFeNH_2^+$	$^4A''$	1.769	1.531	1.022 (2)		88.0	119.0 (2)	109.0	±68.6
	$^6A'$	1.875	1.590	1.021, 1.022		132.3	129.2, 122.0	108.8	0, 180
	$^4A'$	1.770	1.559	1.022 (2)		83.7	119.2 (2)	109.5	±69.3
	$^6A''$	2.153	1.581	1.025 (2)		156.6	127.4, 124.4	108.1	0, 180
TS2	^4A	1.751	1.861, 1.812	1.032, 1.472	0.932	48.0, 76.7	125.4	101.9	90.6, 83.5
	$^6A'$	1.788	1.756, 1.760	1.023, 1.422	1.046	47.2, 81.9	176.3	118.4	180.0
	$^6A''$	1.952	1.758, 1.834	1.025, 1.441	1.042	44.6, 78.2	176.0	120.7	180.0
$(H_2)FeNH^+$	$^6A_1$	1.736	1.907 (2)	1.020	0.773	168.3(2)	180.0		0, 180
	$^4B_1$	1.712	2.001 (2)	1.021	0.767	169.0(2)	180.0		0, 180
	$^4B_2$	1.711	2.001 (2)	1.020	0.767	169.0(2)	180.0		0, 180
	$^6B_1$	1.861	1.956 (2)	1.021	0.770	168.6(2)	180.0		0, 180
	$^6B_2$	1.854	2.006 (2)	1.020	0.765	169.0(2)	180.0		0, 180
	$^4A_2$	1.762	1.838 (2)	1.018	0.792	167.6(2)	180.0		0, 180
	$^6A_2$	1.878	4.100 (2)	1.039	0.743	174.8(2)	180.0		0, 180

[a] Bond lengths in Å. Bond angles in °. All geometries are calculated at the B3LYP/6-311+G* level. Degeneracies in parentheses.

well in excess of the experimental value. In the following discussion, B3LYP//B3LYP values will all be treated in the former manner as this yields thermochemistry in better agreement with the experiments and CCSD(T) calculations.

4.2. Fe^+–NH_2

$D_0(Fe^+–ND_2)$ can be obtained from the thresholds for reaction 2 by using the relationship, $D_0(Fe^+–ND_2) = D_0(ND_2–D) – E_0(2)$. This yields $D_0(Fe^+–ND_2) = 2.7 \pm 0.3$ and 2.91 ± 0.15 eV from the ^6D and ^4F cross sections, respectively, values within experimental error of one another. These values are also nicely consistent with a value obtained from the reaction $Fe_2^+ + ND_3 \rightarrow FeND_2^+ + FeD$, 2.88 ± 0.18 eV [2].[1] Using vibrational frequencies calculated here, Table 4, we can correct the weighted average of the latter two values for zero point energy effects (0.020 eV) to find $D_0(Fe^+–NH_2) = 2.88 \pm 0.12$ eV. This value agrees well with

[1] This value has been adjusted to 0 K thermochemistry.

the bracket established by Buckner and Freiser using chemical reactivity studies, $2.38 < D_{298}(Fe^+–NH_2) < 3.43$ eV [22]. These values are somewhat below a preliminary value from our group, 3.20 ± 0.10 eV [45], but a reexamination of the previous data (both SI and DC/FT) shows them to be comparable to the present data but with much more scatter. In addition, it was believed at the time that iron ions cooled in the flow tube were in the $Fe^+(^6D)$ state with little or no ^4F state present, a result that the present analysis clearly shows is incorrect. Thus the difference between the present and preliminary values corresponds closely to the $Fe^+(^4F)$ excitation energy.

The only previous calculation on the $FeNH_2^+$ species appears to be the B3LYP/DZVP$_{opt}$ calculations of Chiodo et al. [20], however, these authors provide only energetics and no structural information. They find a bond energy of 3.23 eV, whereas our ground state has a bond energy of 2.94 eV (2.89) at the CCSD(T)//B3LYP (B3LYP//B3LYP) levels (including corrections for zero point energies and the spin-orbit levels of the Fe^+ asymptote). The latter values are in good agreement with the present experimental value. Qualitatively, we expect that NH_2 can bond to Fe^+ by forming a covalent bond and then augmenting this by donating the lone pair of electrons on nitrogen to the metal center [45]. Because all of the metal orbitals are at least singly occupied, this leads to an effective bond order of 1.5, consistent with the relative bond energies of Fe^+–H and Fe^+–NH_2. Consistent with this qualitative picture, our calculations find a quintet ground state with $^5A_1$ and $^5A''$ states essentially degenerate (calculations at the B3LYP/6-311+G** and B3LYP//B3LYP levels find that the $^5A_1$ state is lower by 0.035 and 0.027 eV, respectively, whereas the CCSD(T)//B3LYP calculations give $^5A''$ as the ground state by 0.014 eV, Table 5). The $^5A_1$ state has C_{2v} symmetry and a valence electron configuration of $(1a_1)^2(1b_2)^2(2a_1)^2(1b_1)^2(3a_1)^2(1a_2)^1(2b_2)^1(4a_1)^1(2b_1{}^*)^1$, where the $1a_1$ and $1b_2$ are the NH_2 bonding orbitals, the $2a_1$ and $1b_1$ are the Fe–N σ and π bonding orbitals, the $3a_1$ and $1a_2$ are the 3dδ (x^2–y^2 and xy) nonbonding orbitals, the $2b_2$ is the 3dπ (xz) in-plane orbital (essentially nonbonding), the $4a_1$ is a 4s–3dσ (z^2) hybrid orbital (essentially nonbonding), and the $2b_1{}^*$ is the 3dπ (yz) out-of-plane antibonding orbital. The $^5A''$ state moves an electron from the $3a_1$ to the $1a_2$ orbital (both nonbonding 3dδ orbitals), which explains why these states are nearly degenerate, although the difference does lead to distorting from C_{2v} symmetry (dihedral angle of 176.8°, Table 6). Imposing C_{2v} symmetry on the $^5A''$ state does not change the energy appreciably (<0.001 eV at the B3LYP/6-311+G* level), but the umbrella motion (260 cm^{-1} in the $^5A''$ state) becomes imaginary (−398 cm^{-1}) for the $^5A_2$ state, Table 4. It seems possible that higher levels of theory would lead to a minimum at the C_{2v} geometry.

A number of triplet excited states were also found with symmetries of $^3B_2$, $^3A_2$, $^3B_1$, and $^3A_1$ and excitation energies of 0.967 (1.220), 1.181 (0.877), 1.357 (0.990), and 1.400 eV (1.148), respectively, for CCSD(T)//B3LYP (B3LYP//B3LYP) calculations. The low-lying $^3B_2$ state has an electronic configuration of $(3a_1)^2(1a_2)^2(2b_2)^1(4a_1)^1$, consistent with a Fe–N double bond, but correlates with Fe^+ in its ^4F excited state and has less exchange energy than the ground state. We also located several excited quintet states, $^5B_1$, $^5B_2$, $^5A_2$, and $^5A_1$ having excitation energies of 1.864, 4.606, 4.729, and 4.844 eV calculated only at the B3LYP//B3LYP level. The relatively low-lying $^5B_1$ state has an electron configuration in which the electron in the $2b_1{}^*$ orbital of the $^5A_1$ ground state is promoted to a $5a_1{}^*$ orbital, the antibonding σ orbital.

4.3. Fe^+–NH

The $D_0(Fe^+–NH)$ bond energy can be obtained from the CID reactions 6 and 8, where the desired BDE equals the threshold observed. These reactions have thresholds of 3.04 ± 0.15 and 3.1 ± 0.3 eV, in good agreement with one another. However, CID of strongly bound, small molecules often provides thresholds in excess of the true bond energy because collisional energy transfer is inefficient in such systems [47,48]. Fortunately, the $FeNH^+$ bond energy can also be derived from reactions 9 and 10, which interrelate the thermochemistry for $FeNH^+$ and $FeNH_2^+$, and also reaction 11, which couples the bond energies of $FeNH^+$ and FeD^+. For example, the threshold for reaction 10 is given by the relationship $E_0(10) = D_0(Fe^+–NH) - D_0(Fe^+–ND_2) + D_0(N–H) - D_0(N–D_2)$. Using $D_0(Fe^+–ND_2) = 2.90 \pm 0.12$ eV derived above and the literature thermochemistry in Table 2, this gives $D_0(Fe^+–NH) = 2.78 \pm 0.16$ eV. An analogous sequence for reaction 9 yields $D_0(Fe^+–NH) = 2.73 \pm 0.13$ eV. These two values presume that the thresholds of reactions 9 and 10 are the thermodynamic thresholds and not limited by a barrier in excess of the product asymptote, an assumption that will be checked below. If this assumption is unwarranted, then the $E_0(9)$ and $E_0(10)$ values are upper limits to the true thermochemistry, meaning that the derived $FeNH^+$ bond energies are also upper limits. For reaction 11, the endothermicity is given by $E_0(11) = D_0(Fe^+–NH) - D_0(Fe^+–D) + D_0(D_2) - D_0(HN–D)$, which leads to $D_0(Fe^+–NH) = 2.81 \pm 0.21$ eV. All three values are in good agreement and have a weighted average of 2.76 ± 0.09 eV, considerably below the CID values.

Both the 2.76 ± 0.09 and 3.04 ± 0.15 eV values for $D_0(Fe^+–NH)$ agree with the rather broad bracket established by Buckner and Freiser using chemical reactivity studies: $1.78 < D_{298}(Fe^+–NH) < 3.51$ eV [22], but only the former value agrees with the photodissociation value of 2.65 ± 0.22 eV [22,24]. Probably the best value in the literature comes from a measurement by Brönstrup et al. of the $FeO^+ + NH_3 \rightleftarrows FeNH^+ + H_2O$ equilibrium in which $\Delta H_{298} \approx \Delta G_{298} = -0.22 \pm 0.03$ eV was obtained [21]. They reported $D_{298}(Fe^+–NH) = 2.99 \pm 0.09$ eV, which agrees well with the present CID values, but the derivation of this value appears to utilize older thermochemistry for the NH radical. Here we correct their 298 K enthalpy

of reaction to a 0 K value of $\Delta H_0 = -0.24 \pm 0.04$ eV using H_{298}–H_0 values of 8.87, 10.04, 10.99, and 9.90 kJ/mol for FeO^+, NH_3, $FeNH^+$, and H_2O, respectively. Values for NH_3 and H_2O are taken from the JANAF tables [53] and those for FeO^+ and $FeNH^+$ are calculated using molecular constants calculated as described above. Using $D_0(FeO^+) = 3.47 \pm 0.06$ eV (the value that Brönstrup et al. also used) [54], $D_0(O{-}H_2) = 5.034 \pm 0.001$ eV [53] and $D_0(NH{-}H_2) = 4.103 \pm 0.011$ eV (Table 2), we obtain $D_0(Fe^+{-}NH) = 2.54 \pm 0.06$ eV–$\Delta H_0 = 2.78 \pm 0.09$ eV. This is in excellent agreement with the values obtained from reactions 9–11 and with the photodissociation value. Note that this agreement is consistent with the thresholds of reactions 9 and 10 being the true thermodynamic values, which helps confirm the relative energetics of $FeNH^+$ and $FeNH_2{}^+$ derived here.

Theoretical calculations by Brönstrup et al. (B3LYP/6-311+G* geometry optimizations followed by single point calculations at the MR-ACPF/CASSCF level) [21] and our studies agree that the ground state of $FeNH^+$ is $^6\Sigma^+$. Chiodo et al. (B3LYP/DZVP$_{opt}$ geometry and single point energy calculations) [20] report the ground state to be $^6A'$, but no details of the geometry are presented and it seems likely that they simply did not converge this geometry to $C_{\infty v}$. Our calculations (Table 6) reproduce the ground state geometry reported by Brönstrup et al. [21], r_e(Fe–NH) = 1.725 Å, r_e(FeN–H) = 1.020 Å, and ∠(FeNH) = 180°, as well as those for the $^4A'$ excited state, r_e(Fe–NH) = 1.731 Å, r_e(FeN–H) = 1.026 Å, and ∠(FeNH) = 141°. We obtain a somewhat different geometry for the $^2\Delta$ excited state, r_e(Fe–NH) = 1.756 Å, r_e(FeN–H) = 1.030 Å, and ∠(FeNH) = 180°, compared to values of 1.713 Å, 1.028 Å, and 180° obtained by Brönstrup et al. [21]. We also located a $^4A''$ state with r_e(Fe–NH) = 1.726 Å, r_e(FeN–H) = 1.025 Å, and ∠(FeNH) = 146° (which is very similar to the $^4A'$ state), and a $^2\Sigma^+$ state with r_e(Fe–NH) = 1.711 Å, r_e(FeN–H) = 1.028 Å, and ∠(FeNH) = 180°. Excitation energies for the $^4A''$, $^4A'$, $^2\Delta$, and $^2\Sigma^+$ states are found to be 0.06 (0.08), 0.07 (0.09), 2.47 (0.69), and 3.27 eV (1.59), respectively, at the CCSD(T)//B3LYP (B3LYP//B3LYP) levels, Table 5. The B3LYP calculations agree reasonably well with the excitation energies reported by Brönstrup et al. [21], 0.14 and 0.51 eV for the $^4A'$ and $^2\Delta$ states, respectively.

Brönstrup et al. [21] discuss the bonding in $FeNH^+$ in some detail, but it is worth noting the valence electronic configuration here. The $^6\Sigma^+$ ground state has a $(1\sigma)^2(2\sigma)^2(1\pi)^4(1\delta)^2(3\sigma)^1(2\pi^*)^2$ configuration where the 1σ is NH bonding, the 2σ and 1π are Fe–N bonding, the 1δ is Fe(3d) nonbonding, the 3σ is a nonbonding Fe(4s–3dσ) hybrid orbital, and the $2\pi^*$ is Fe–N antibonding. Note that this means that the effective bond order in this molecule is approximately 2. Like the $^5A_1$ ground state of $FeNH_2{}^+$, the exchange energy of the high spin state is more favorable than not populating the antibonding $2\pi^*$ obitals, but the energetic trade off is close, such that the quartet states have low excitation energies. The $^4A'$ and $^4A''$ excited states have configurations of $(1\sigma)^2(2\sigma)^2(1\pi)^4(1\delta)^3(3\sigma)^1(2\pi^*)^1$ before distortion from a linear geometry and are distinguished by which 1δ orbital is doubly occupied, explaining why the geometries are so similar; however, emptying a single $2\pi^*$ orbital allows the molecule to bend in this direction. If both $2\pi^*$ orbitals are emptied, the resultant $^2\Delta$, $(1\sigma)^2(2\sigma)^2(1\pi)^4(1\delta)^3(3\sigma)^2$, and $^2\Sigma^+$, $(1\sigma)^2(2\sigma)^2(1\pi)^4(1\delta)^4(3\sigma)^1$, states return to linear geometries. As calculated by Brönstrup et al. [21], the potential energy surfaces for bending the molecule in all of these states are quite shallow. Note that the bond orders of the quartet and doublet states are 2.5 and 3, presuming the 3σ orbital is nonbonding. These states still lie higher in energy than the sextet state with a lower bond order presumably because of favorable exchange energy and the need to couple with an excited state of Fe^+.

Our calculations find a bond energy for $Fe^+{-}NH$ of 2.40 eV (2.43), in reasonable agreement with the value obtained by Brönstrup et al. [21] of 2.51 eV (2.46 eV if corrected for the spin-orbit levels of the $Fe^+(^6D)$ state). Using B3LYP/DZVP$_{opt}$, Chiodo et al. [20] calculate a threshold of 1.34 eV for the reaction $Fe^+ + NH_3 \rightarrow FeNH^+ + H_2$. These authors do not report any auxiliary thermochemistry for ammonia, so we combine this energy with our B3LYP/6-311+G* (a comparable level of theory) value for $D_0(NH{-}H_2)$ to find a $D_0(Fe^+{-}NH)$ bond energy of 2.51 eV (which again should probably be lowered by 0.05 eV for the spin-orbit splitting in Fe^+). All the theoretical values are in reasonable agreement with one another but lie somewhat lower than the experimental values of 2.76 ± 0.09 (present study) and 2.78 ± 0.09 eV (revised equilibrium value). Note that theory agrees better with these lower experimental values than with the values near 3 eV.

4.4. Bond energy–bond order correlation

Further understanding of the $FeNH_2{}^+$ and $FeNH^+$ bond energies can be obtained by comparing these to the bond strengths of organic analogues, specifically CH_3NH_2 ($D_0 = 3.61$ eV) [55] and CH_2NH (D = 6.55 eV) [21], respectively. To calibrate these comparisons, we also include the singly bonded species $Fe^+{-}H$ and $Fe^+{-}CH_3$ versus $CH_3{-}H$ and $CH_3{-}CH_3$, as well as the doubly bonded $Fe^+{=}CH_2$ and $Fe^+{=}O$ versus $CH_2{=}CH_2$ and $CH_2{=}O$. These various bond energies are compared in Fig. 6. As previously pointed out by Brönstrup et al. [21], the $Fe^+{-}NH$ bond energy is weaker than the isovalent $Fe^+{-}CH_2$ and $Fe^+{-}O$ bond energies by an amount proportional to the bond energies of $CH_2{-}NH$ versus $CH_2{-}CH_2$ and $CH_2{-}O$. In some respects, this is surprising as the ground state $FeNH^+$ ($^6\Sigma^+$) species is linear, implying formation of a triple bond, but the double occupation of the $2\pi^*$ antibonding orbitals reduces the effective bond order to 2 (see above). The low-lying $^4A''$ and $^4A'$ excited states have bent geometries, consistent with formation of a double bond. Although the $CH_3{-}L$ bond energies for L=H, CH_3, and NH_2 are all comparable, consistent with analogous single covalent bonds, the bonds of these species to Fe^+ increase from H

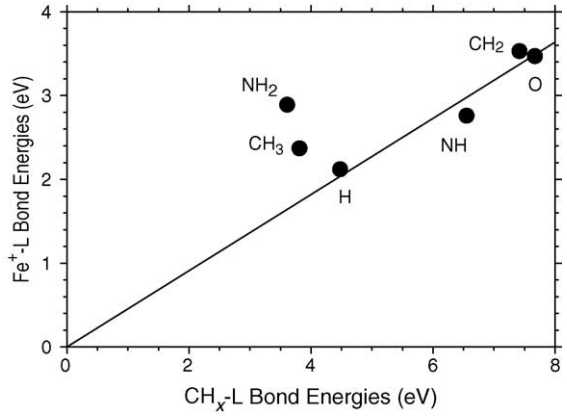

Fig. 6. Correlation of experimental Fe^+—L (L = H, CH_3, NH_2, NH, CH_2, and O) bond energies with organic analogues, specifically, CH_3—L for the first three ligands and CH_2—L for the latter three.

to CH_3 to NH_2. As discussed previously [45], the Fe^+–CH_3 bond energy is enhanced relative to Fe^+–H by the larger polarizability of the methyl ligand compared to a hydrogen atom. This work also points out that NH_2 bonds to transition metal ions can be enhanced by donation of the lone pair of electrons on the amine to orbitals on the metal ion, thereby forming a dative bond [45]. Periodic trends in the enhancement observed for other metal ions find an average enhancement of 1.24 ± 0.28 eV for a full dative bond. For metals ions to the right of the periodic table, the acceptor orbital on the metal is singly occupied, such that the enhancement is observed to be approximately half this value. The value determined here by comparing $D_0(Fe^+–CH_3)$ versus $D_0(Fe^+–NH_2)$ is 0.51 ± 0.13 eV, in good agreement with this prediction and comparable to the differences observed for $M^+–CH_3$ versus $M^+–NH_2$ bond energies with M=Co, Ni, and Cu [45]. We have also found that the bond energies for iron clusters show a similar trend, i.e., $D_0(Fe_x^+–ND_2)$ exceed $D_0(Fe_x^+–D)$ by an average of 0.8 ± 0.1 eV for $x = 2$–6 [3], in good agreement with the 0.72 ± 0.16 eV difference found here for $x = 1$.

5. Potential energy surfaces and reaction mechanism

5.1. Potential energy surfaces

The potential energy surface for the reaction of Fe^+ with ammonia has been discussed previously by Chiodo et al. [20], but is worth revisiting in light of the state-specific experimental information available here. Qualitatively, the potential energy surface calculated by Chiodo et al. agrees with that found here, but the present calculations are performed at a higher level of theory. Energies relative to the ground state $Fe^+(^6D_{9/2}) + NH_3$ reactants at several levels of theory are provided in Table 7 and calculated from information in Table 5. Fig. 7 shows the overall surfaces calculated at the CCSD(T)/6-311++G(3df,3p)//B3LYP/6-311+G* level. Table 6 and Fig. 8 provide details of the geometries of the intermediates and transition states along both the sextet and quartet surfaces.

All calculations agree that interaction of Fe^+ with ammonia initially leads to a strongly bound $FeNH_3^+$ adduct formation, Fig. 7. One anticipates that the excited $Fe^+(^4F, 3d^7)$ ion should be able to bind ammonia more strongly than ground state $Fe^+(^6F, 4s^13d^6)$ because the empty 4s orbital provides a much better acceptor for the nitrogen lone pair of electrons. Most levels of theory, Table 7, find that the $^4A_1$ state is the ground state, but the CCSD(T)//B3LYP calculations find that the ^6E state lies only 0.01 eV higher in energy, and the MCPF calculations of Langhoff et al. [56] find a ^6E ground state lying 0.22 eV below a $^4A_2$ state. (This state specification seems odd as s, p, and d orbitals do not have

Table 7
Calculated energies (eV) for $[Fe,N,3H]^+$ reactants, intermediates, transition states, and products[a]

Species	State	B3LYP/6-311+G*	B3LYP/6-311++G(3df,3p)	CCSD(T)/6-311++G(3df,3p)	B3LYP/DZVP$_{opt}$[b]	Exp
$Fe^+ + NH_3$	^6D	0.518	0.512	0.052	0.00	
	^4F	0.300	0.300	0.554	0.54	
$FeNH_3^+$	$^4A_1$	−1.972	−1.851	−1.760	−2.02	−1.90 ± 0.12
	^6E	−1.451	−1.326	−1.751	−1.81	
TS1	^4A	0.146	0.179	0.138	−0.17	
	$^6A''$	1.128	1.218	1.333	0.81	
$HFeNH_2^+$	$^4A''$	−0.046	0.011	0.194	−0.28	
	$^6A'$	0.044	0.140	0.252	−0.24	
TS2	^4A	1.992	1.908	1.928	1.60	1.60 ± 0.09
	$^6A'$	2.018	1.984	1.989	1.78	
$(H_2)FeNH^+$	$^6A_1$	0.931	0.957	1.015	0.78	
	$^4B_1$	1.136	1.131	1.360	0.97	
$FeNH^+ + H_2$	$^6\Sigma^+$	1.445	1.556	1.571	1.34	1.34 ± 0.08
	$^4A'$	1.559	1.623	1.619	1.64	
$FeH^+ + NH_2$	$^5\Delta$	2.449	2.457	2.234	2.13	2.51 ± 0.06
$FeNH_2^+ + H$	$^5A''$	1.497	1.607	1.509	1.42	1.75 ± 0.12
	$^5A_1$	1.462	1.580	1.523		

[a] Geometries of all species calculated at the B3LYP/6-311+G* level. Energies include zero point energy corrections calculated at the B3LYP/6-311+G* level.
[b] Ref. [20].

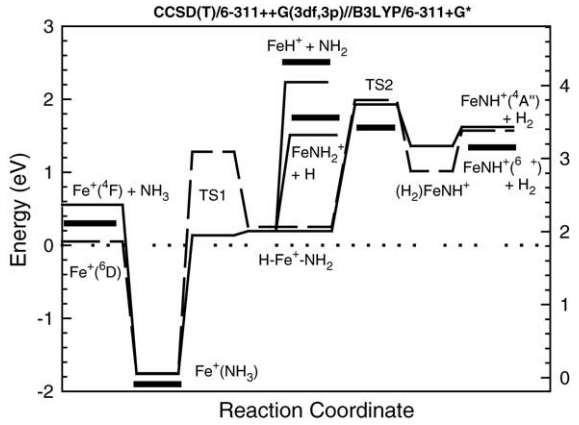

Fig. 7. Theoretical potential energy diagram for interaction of Fe^+ with ammonia obtained at the CCSD(T)/6-311++G(3df,3p)//B3LYP/6-311+G* level of theory. Solid lines show surfaces of quartet spin, whereas the dashed lines show those of sextet spin. Bold lines indicate experimental values (Table 7).

a_2 symmetry in the C_{3v} point group.) In all cases, the calculated energy of the ground state species is in reasonable agreement with the experimental bond energy for Fe^+–NH_3 [57], Table 7. It can also be noted that the diabatic (spin-conserving) bond energy calculated at the CCSD(T)//B3LYP level for the $^4A_1$ state is 2.31 eV (=1.760 + 0.554, Table 7), which corresponds to an adiabatic bond energy of 2.01 eV if the $Fe^+(^4F) + NH_3$ asymptotic value is adjusted to the experimental value of 0.30 eV. The geometries calculated here for both states, Fig. 8 and Table 6, are comparable to those found by Chiodo et al.; r_e(Fe–N) = 2.322 and 2.019 Å and ∠(FeNH) = 112.5 and 112.1° for ^6E and $^4A_1$, respectively; as well as Langhoff et al.: r_e(Fe–N) = 2.186 and 2.083 Å for ^6E and $^4A_2$, respectively.

Reaction with ammonia proceeds by oxidative addition of an N–H bond to Fe^+. Calculations indicate that the energies of the transition states (TS1) for this process differ appreciably on the sextet and quartet surfaces, Fig. 7. This can be understood using simple molecular orbital (MO) arguments that have been detailed elsewhere [4–7]. These arguments demonstrate that the difference in reactivity of $Fe^+(^6D)$ and $Fe^+(^4F)$ can be attributed to the electron configurations of these states, $4s^13d^6$ and $3d^7$, respectively. The 4s is the largest orbital on the metal ion and therefore the first to interact with an NH bond in ammonia. This 4s orbital mixes with the σ(NH) bonding orbital to form bonding and antibonding MOs. Because the σ(NH) orbital is doubly occupied, the bonding MO is doubly occupied and the occupation of the antibonding MO tracks with the population of the 4s orbital. When the 4s is occupied (as for ^6D), the antibonding MO is occupied, leading to a repulsive interaction that yields the high lying TS1 ($^6A''$) transition state, Fig. 8. In contrast, in reaction of the $Fe^+(^4F)$ state, the antibonding MO remains unoccupied leading to a much more favorable interaction such that at the CCSD(T)//B3LYP (B3LYP//B3LYP) level of theory the TS1 (^4A) transition state lies 1.20 eV (1.04) lower in energy than TS1 ($^6A''$) (0.98 eV in the calculations of Chiodo et al.).

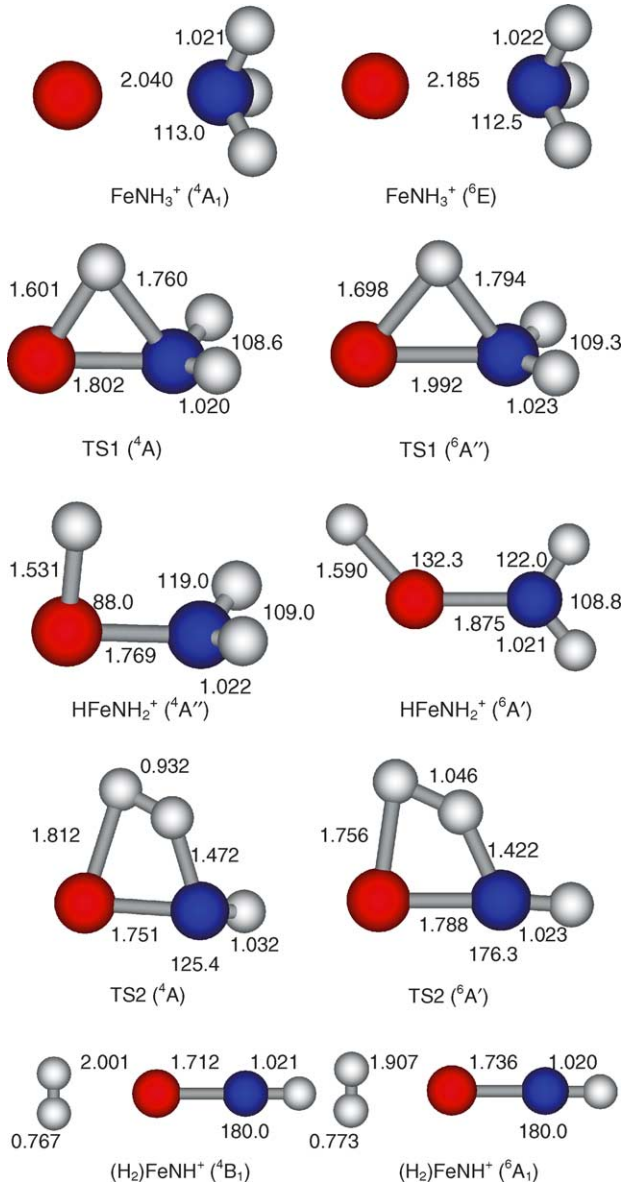

Fig. 8. Geometries for all intermediates and transition states involved in the reaction of $Fe^+(^6D, ^4F)$ with ammonia calculated at the B3LYP/6-311+G* level. Bond distances shown are in Å and angles are in °.

Indeed, although the energy of the quartet transition state is calculated to lie above the ground state H–Fe^+–NH_2 intermediate by 0.19 eV at the B3LYP level where the geometry optimizations are performed and 0.17 eV at the B3LYP//B3LYP level (values comparable to the 0.10 eV obtained by Chiodo et al.), it is lower by 0.06 eV at the CCSD(T)//B3LYP level of theory, Fig. 7 and Table 7. Presumably, geometry optimizations at this higher level of theory would restore the energy of TS1 to be higher than the intermediate, but clearly the barrier relative to the intermediate is small. Despite this large difference in energy, the structures of the ^4A and $^6A''$ TS1 species are qualitatively similar, although the Fe–N and Fe–H bond lengths are appreciably longer in the sextet state. Chiodo et al. find a similar result at their B3LYP/DZVP level of theory, but

the Fe–N bond lengths are identical at the B3LYP/DZVP$_{opt}$ level.

Calculations indicate that the H–Fe^+–NH_2 intermediate is a ground state quartet ($^4A''$) but the analogous sextet state ($^6A'$) is low-lying, 0.06 eV (0.13) higher at the CCSD(T)//B3LYP (B3LYP//B3LYP) level, whereas Chiodo et al. find a difference of 0.04 eV. ($A\ ^6A''$ state was also found lying 0.56 eV above the $^4A''$ state at the B3LYP//B3LYP level.) The geometries of the two spin states differ dramatically, Fig. 8, in agreement with the results of Chiodo et al. Although both species have C_s symmetry, in the $^4A''$ state, the Fe–H bond lies perpendicular to the NH_2 ligand, whereas the $^6A'$ and $^6A''$ states are planar. It is interesting to note that the $^4A''$ state has a Fe–N bond that is actually shorter than that in the $FeNH_2^+$ ($^5A''$) species, and the Fe–H bond is shorter than in FeH^+ ($^5\Delta$). Apparently, this species can be viewed as binding the hydrogen ligand to one of the $2\pi^*$ orbitals of $FeNH_2^+$ ($^5A''$), which thereby removes antibonding character from the Fe–N bond. In contrast, the high spin of the $^6A'$ and $^6A''$ states requires that the hydrogen atom add its electron to a high-lying unoccupied antibonding orbital of $FeNH_2^+$ ($^5A''$), leading to longer Fe–N and Fe–H bonds than in $FeNH_2^+$ and FeH^+.

The $HFeNH_2^+$ intermediate is clearly the gateway to three different products: FeH^+, $FeNH_2^+$, and $FeNH^+$. FeH^+ and $FeNH_2^+$ can be produced by simple bond cleavage from this intermediate, Fig. 7, which explains the strong competition between these two channels observed experimentally. The dehydrogenation reaction forming $FeNH^+(^6\Sigma^+) + H_2$ also must occur through this intermediate by way of transition state TS2. The quartet and sextet surfaces parallel one another in this region of the potential energy surface such that the CCSD(T)//B3LYP calculations find TS2 ($^6A'$) lies 0.06 eV above TS2 (^4A). Our B3LYP energies are comparable to this, Table 7, whereas Chiodo et al. calculate a difference of 0.18 eV. In both cases, a four-centered transition state involving an incipient H–H bond is formed, Fig. 8, as also found by Chiodo et al. Clearly the geometries of the FeNH portion of the TS2 transition states are consistent with the quartet and sextet states of the $FeNH^+$ products, Table 6 and Figs. 5 and 8. Significantly, TS2 (^4A) is located 0.36 eV (0.35) (CCSD(T)//B3LYP and B3LYP//B3LYP) above the energy of the $FeNH^+ + H_2$ products, whereas Chiodo et al. find a difference of 0.26 eV. In other words, theory predicts that there is barrier to formation of the $FeNH^+ + H_2$ products from $Fe^+ + NH_3$ in excess of the endothermicity of this channel.

Once over TS2, the system forms a $(H_2)FeNH^+$ intermediate, which is a dihydrogen adduct of the $FeNH^+$ product ion. The geometries of these species on the quartet and sextet surfaces are similar, Fig. 8, which is somewhat surprising as both species have a linear FeNH bond angle, in contrast to the geometry of the $FeNH^+$ ($^4A''$) state, Fig. 5. However, Brönstrup et al. calculate that the distortion energy for bending $FeNH^+$ to a linear species on the quartet surface is only 0.09 eV [21]. Presumably, this distortion leads to the higher energy of the quartet state compared to the sextet state, which is calculated to lie lower in energy than the $^4B_1$ state by 0.34 eV (0.17) at the CCSD(T)//B3LYP (B3LYP//B3LYP) levels of theory, comparable to the difference found by Chiodo et al. of 0.19 eV. Several other states, $^4B_2$, $^6B_1$, $^6B_2$, $^4A_2$, $^6A_2$, were also investigated at the B3LYP/6-311+G* level of theory and were found to lie 0.23 to over 4.7 eV higher in energy, Table 5. Elimination of H_2 from the $(H_2)FeNH^+$ intermediates occurs without a barrier to form the $FeNH^+ + H_2$ products on both sextet and quartet surfaces. This requires energies of 0.56 eV (0.60) on the sextet surface and 0.26 eV (0.49) on the quartet surface at the CCSD(T)//B3LYP (B3LYP//B3LYP) levels of theory. Chiodo et al. calculate values of 0.56 and 0.66 eV for the sextet and quartet surfaces, respectively.

5.2. Reaction mechanism – comparison to experiment

Given the potential energy surface in Fig. 7, the state-specific reactivity of $Fe^+(^6D, ^4F)$ with ammonia and the reverse reaction of $FeNH^+$ with D_2 can be understood. Reaction of $Fe^+(^4F)$ can form both the $Fe^+(NH_3)$ and $HFeNH_2^+$ intermediates exothermically. From the latter, endothermic formation of $FeNH_2^+ + H$ begins promptly at the thermodynamic threshold, as does $FeH^+ + NH_2$. Because these two channels share the common $HFeNH_2^+$ intermediate, they compete strongly with one another. The $FeH^+ + NH_2$ channel dominates at higher energies because angular momentum is conserved more easily for these products than for the $FeNH_2^+ + H$ products [8–10,58,59]. (Briefly, this is primarily because the reduced mass of the $FeNH_2^+ + H$ channel, 1.0 amu, is much smaller than that for the $Fe^+ + NH_3$ reactants, 13.0 amu, which is comparable to that for the $FeH^+ + NH_2$ products, 12.5 amu.) Note that calculations indicate that the barrier to $FeNH^+ + H_2$ formation, TS2, actually lies above the energy calculated for the $FeNH_2^+ + H$ channel, although experimental information (Tables 2 and 3) suggests that the barrier corresponding to TS2 is 0.15 ± 0.15 eV below the asymptotic energy of the $FeNH_2^+ + H$ product channel, Table 7. In either event, TS2 is a tight transition state that is entropically much less favorable than the loose transition state leading to $FeND_2^+ + D$, such that $FeND^+ + D_2$ is not observed as a product in the reaction of Fe^+ with ND_3, Figs. 1 and 2.

Reaction of ammonia with $Fe^+(^6D)$ is much less efficient than with $Fe^+(^4F)$, Fig. 2, an observation that has also been made in the state-specific reactions of Fe^+ with CH_4 and H_2O [15,17]. Cross sections for formation of FeD^+ from both states have comparable shapes and thresholds displaced by the appropriate energy difference between the reactant states, Table 1, but the magnitude is about a factor of six smaller for the ^6D state compared to the ^4F state. An even larger difference is observed for the $FeND_2^+$ product cross sections where the peak in the cross sections differ by a factor of about 20, but in addition, the ^6D cross section rises much more slowly, indicating a much less efficient process. This change in the cross section shape suggests that $FeND_2^+$ is formed primarily by crossing from the sextet to the quartet surface, which introduces an energy dependence of approximately

$E^{-1/2}$ [60] and leads to the slower onset of reactivity. This seems reasonable because the energy of TS1 ($^6A''$) is not much lower than that for $FeNH_2^+ + H$: 1.333 eV (1.283) versus 1.523 eV (1.580) above the $Fe^+(^6D) + NH_3$ reactants as calculated at the CCSD(T)//B3LYP (B3LYP//B3LYP) levels of theory. The observation that the FeD^+ cross section does not exhibit the same slow onset as $FeND_2^+$ may indicate that this high-energy product is also accessible via more direct reaction pathways, e.g., a collinear interaction of $Fe^+(^6D)$ with an ND bond.

Results for the reverse reaction of $FeNH^+ + D_2$, Fig. 4, can also be addressed in detail utilizing the potential energy surface of Fig. 7. Although formation of $Fe^+ + NHD_2$ is exothermic, this product is not observed until a barrier of 0.27 ± 0.05 eV is first surmounted, Table 1. The zero point energy correction to this barrier height (Table 4) is 0.01 eV, such that the barrier for the [Fe, N, 3H]$^+$ system is 0.26 ± 0.05 eV. This energy is in reasonable agreement with values calculated here, 0.36 eV (0.35) at the CCSD(T)//B3LYP (B3LYP//B3LYP) levels, or by Chiodo et al., 0.25 eV, presuming the barrier corresponds to TS2 (^4A). If the system remains on the sextet surface, the calculated barriers are slightly higher at 0.42 (0.43) and 0.43 eV, respectively. Similar barriers in the reverse reaction have been reported for the related isoelectronic systems, $FeO^+ + D_2$, ~0.6 eV [17], and $FeCH_2^+ + D_2$, ~0.4 eV [16]. For these two systems, the theory of Chiodo et al. predicts barriers of 0.15 eV (0.46 if spin conserving) and 0.46 eV (both adiabatic and spin-conserving), respectively, whereas calculations by Musaev et al. [61] overestimate this barrier height in the CH_4 system: ~0.9 eV.

The calculations indicate clearly that the barrier for reaction 7 corresponds to the four-centered transition state, TS2, which is surmounted in order to form the D–Fe^+–NHD intermediate. Clearly, this intermediate can decompose into $FeNHD^+ + D$ as well as $FeD^+ + NHD$, which experiment indicates occur at their thermodynamic thresholds (see discussion above). Thus, experimentally, it is found that the energy of the $FeNH_2^+ + H$ asymptote must lie above but very close to TS2 (i.e., the threshold for formation of $FeNHD^+ + D$ is 0.11 ± 0.07 eV higher than the barrier leading to $Fe^+ + NHD_2$, Table 1). Note that both the present theory and the results of Chiodo et al. [20] find the TS2 barrier has an energy in excess of the $FeNH_2^+$ asymptote, Table 7. This appears to be primarily a limitation in the ability of theory to properly calculate the energetics of $FeNH^+$ (and thus its related adduct and transition state), as the bond energy for this species is underestimated, Table 3.

Further information can be gleaned from a careful consideration of the results shown in Fig. 4. First, as noted above, the formation of $Fe^+ + NHD_2$ appears to decrease above about 1.5 eV because of competition with the $FeNHD^+ + D$ product channel. This naturally occurs because these processes share the D–Fe^+–NHD intermediate, and the competition indicates that elimination of D at higher kinetic energies is entropically favored compared to passing over TS1 to form the $Fe^+(NHD_2)$ intermediate. Second, formation of $FeND_2^+$ requires a hydrogen/deuterium scrambling process as this species is not directly formed from the D–Fe^+–NHD intermediate. Two possible mechanisms can be envisioned: (a) the system passes back over TS2 to form $(HD)FeND^+$, which then returns over TS2 to yield H–Fe^+–ND_2, which can eliminate H, or (b) the system proceeds on to $Fe^+(NHD_2)$ and then activates the NH bond to form H–Fe^+–ND_2. The failure to observe $FeND^+$, which could easily be formed from the $(HD)FeND^+$ intermediate, may suggest the latter mechanism is favored. In either case, the scrambling requires additional steps that become increasingly less likely with increasing energy because of the decreasing lifetime of the initially formed D–Fe^+–NHD intermediate. As can be seen in Fig. 4, the ratio of the magnitudes of the $FeNHD^+$ and $FeND_2^+$ cross sections is about 4 near threshold and increases to about 10 at the peak near 3 eV. Note that in contrast to the results for reaction of Fe^+ with ND_3, the ratio of the FeD^+ and $FeNHD^+$ cross sections favor the iron amide cation. As noted above, angular momentum constraints limit the production of $FeND_2^+$ in the former system, whereas here the reduced mass of the $FeNHD^+ + D$ channel, 2.0 amu, is comparable to that for the $FeNH^+ + D_2$ reactants, 3.8 amu, such that the thermodynamically favored product dominates over the higher energy $FeD^+ + NHD$ products.

6. Conclusion

The potential energy surface for the interaction of iron cations with ammonia is studied both experimentally and theoretically. State-specific reactions of $Fe^+(^6D, {}^4F)$ with ND_3 and the reaction of $FeNH^+ + D_2$ are both studied as a function of kinetic energy. Combined with previous experimental results for the bond energies of FeH^+ [45,50] and Fe^+–NH_3 [57], energies of key products (FeH^+, $FeNH^+$, and $FeNH_2^+$), intermediates, and the rate-limiting transition state (TS2) are quantified. This information is compared to theoretical potential energy surfaces calculated here at several levels of theory and those of Chiodo et al. [20]. We find that $Fe^+(^6D)$ is much less reactive than $Fe^+(^4F)$, which can be explained using simple molecular orbital arguments that are supported by the theoretical potential energy surfaces. Unlike early transition metal ions (Sc^+–V^+) [8,9], but comparable to late ones (Co^+–Cu^+) [10], Fe^+ does not dehydrogenate ammonia, which is shown experimentally and theoretically to be the result of a barrier in excess of the endothermicity of this process attributable to a four-centered transition state, TS2. This system is prototypical for understanding the details of how ammonia interacts with iron clusters [2] and iron surfaces [1].

Acknowledgments

This work is supported by the National Science Foundation, Grant No. CHE-0135517. The authors thank Detlef

Schröder for his insightful review and for pointing out reference 63.

Appendix A. Implications for the bond energy of $FeOH^+$

A referee notes that the bond energy for Fe^+–NH_2 derived here introduces a potential dichotomy with respect to previous work in the literature that relates the $FeOH^+$ and $FeNH_2{}^+$ bond energies through reaction A1, as first observed by Buckner and Freiser [22]

$$FeOH^+ + NH_3 \rightarrow FeNH_2{}^+ + H_2O \quad (A.1)$$

Subsequently, Brönstrup, Schröder, and Schwarz quantified this process as having a rate constant of 2.3×10^{-10} cm^3 $molecules^{-1}$ s^{-1} and an efficiency of 0.1 [62]. The reverse process can also be observed and has a higher efficiency of 0.26, indicating that reaction A1 is endothermic. Although a true equilibrium cannot be established between these two ions in the presence of both H_2O and NH_3, presumed to be because of competing association channels, the authors suggest that the endothermicity of the reaction must be within thermal range. Taking $D_0(Fe^+–OH) = 3.72 \pm 0.10$ eV [63], $D_0(HO–H) = 5.121 \pm 0.003$ eV [53], and $D_0(H_2N–H) = 4.632 \pm 0.011$ eV (Table 2), we find $D_0(Fe^+–NH_2)$ should be somewhat less than 3.23 ± 0.10 eV. A $D_0(Fe^+–NH_2) = 2.88 \pm 0.12$ eV value would give an exothermicity for reaction 12 of 0.35 ± 0.16 eV, which is too large to give a near thermal equilibrium.

Given the results for reaction A1, this means that the bond energy for $FeOH^+$ deserves additional scrutiny. The value cited in [63] is the average of a CCSD(T) calculation (3.69 ± 0.09 eV) [43], a threshold collision-induced dissociation (TCID) value (3.70 ± 0.13 eV) [64], and a preliminary value from our laboratory (3.79 ± 0.12 eV) [45]. The TCID work of Michl and coworkers was one of the earliest threshold studies and did not incorporate a full analysis of the thermal energy content of the ions. Values obtained in this study for $TiOH^+$, VOH^+, $CrOH^+$, $MnOH^+$, and $CoOH^+$ average 0.10 ± 0.05 eV higher than 0 K values from our laboratory [45] and values for $ScOH^+$ and $NiOH^+$ fall lower than our values by 1.36 and 0.60 eV, respectively. Thus, a value of 3.60 ± 0.14 eV is a more reasonable value from this study. The 3.79 ± 0.12 eV value from our laboratory comes from a preliminary analysis of the kinetic energy dependence of the $Fe^+ + CH_3OH \rightarrow FeOH^+ + CH_3$ reaction. This study, which is still not published, appears to suffer from the same difficulties as the preliminary work on the $Fe^+ + NH_3$ reaction noted above, specifically that the Fe^+ state distribution may have been improperly characterized. A potentially more reliable value comes from our published work on the state-specific reactions of $Fe^+(^6D, {}^4F)$ with D_2O [17], directly analogous to the present work with ammonia. There the threshold for formation of $FeOD^+ + D$ from $Fe^+(^4F)$ formed by surface ionization at 2300 K was measured as 1.38 ± 0.22 eV. Given $D_0(DO–D) = 5.212 \pm 0.003$ eV [53] and $E_{el}(2300\,K) = 0.284$ eV, we obtain $D_0(Fe^+–OD) = 3.55 \pm 0.22$ eV, which can be adjusted for zero point energy differences (0.007 eV as calculated here for the $^5A'$ ground state at the B3LYP/6-311+G* level) to $D_0(Fe^+–OH) = 3.54 \pm 0.22$ eV. The average of this value with that adjusted from the Michl TCID study is 3.57 ± 0.14 eV, which we take as our recommended value. Note that if our preliminary value of 3.79 ± 0.12 eV is lowered by the $Fe^+(^4F)$ excitation energy of 0.30 eV, the resulting value is in good agreement with this recommendation. Further, Schröder and Schwarz [63] cite several other experimental values, including 3.17 ± 0.13 eV [65], 3.3 ± 0.2 eV [65], 3.34 ± 0.26 eV [66], and 3.9 ± 0.3 eV [67]. None of these seems particularly definitive, but the latter three values are all within the combined experimental error of 3.57 ± 0.14 eV. Unlike Schröder and Schwarz, we choose not to include the CCSD(T) calculated value of 3.69 eV from Irigoras et al. [43] in our average, largely because our own calculations of this species, performed here at the levels discussed above, provide lower Fe^+–OH bond energies of 3.53 eV (CCSD(T)//B3LYP) and 3.35 eV (B3LYP//B3LYP). Note that the CCSD(T) values calculated here for $D_0(Fe^+–NH_2)$ and $D_0(Fe^+–OH)$, 2.94 and 3.53 eV, respectively, agree very well with our experimental values of 2.88 ± 0.15 and 3.57 ± 0.14 eV, respectively.

Finally, given these experimental values, we find that the endothermicity of reaction 12 is 0.20 ± 0.21 eV, within experimental error of being close to thermoneutral, as observed by Brönstrup et al. [62]. The bond energy for $FeNH_2{}^+$ determined here is also supported by the thresholds for reactions 9 and 10, which provide self-consistent thermochemistry relating $D_0(Fe^+–NH_2) = 2.88 \pm 0.15$ eV and $D_0(Fe^+–NH) = 2.76 \pm 0.09$ and 2.78 ± 0.09 eV [21]. Likewise the discussion (Section 4.4) of the periodic trends in the bond order and the relationship with the $Fe_xNH_2{}^+$ bond energies are less consistent if the value of 3.2 eV is used. Therefore, we think it likely that the literature value for $D_0(Fe^+–OH)$ should be adjusted downwards somewhat, with a recommended value of 3.57 ± 0.14 eV. This deserves further study.

References

[1] G. Ertl, in: J.R. Anderson, M. Boudart (Eds.), Catalysis: Science and Technology, 4, Springer, Berlin, 1983;
G. Ertl, Catal. Rev. -Sci. Eng. 21 (1980) 201;
G. Ertl, in: J.R. Jennings (Ed.), Catalytic Ammonia Synthesis, Plenum Press, New York, 1991, p. 109;
M. Grunze, F. Bozso, G. Ertl, M. Weiss, Appl. Surf. Sci. 1 (1978) 241.
[2] J. Conceição, S.K. Loh, L. Lian, P.B. Armentrout, J. Chem. Phys. 104 (1996) 3976.
[3] R. Liyanage, J.B. Griffin, P.B. Armentrout, J. Chem. Phys. 119 (2003) 8979.

[4] J.L. Elkind, P.B. Armentrout, J. Phys. Chem. 91 (1987) 2037.
[5] P.B. Armentrout, in: D.H. Russell (Ed.), Gas Phase Inorganic Chemistry, Plenum Press, New York, 1989, p. 1.
[6] P.B. Armentrout, in: J.A. Davies, P.L. Watson, J.F. Liebman, A. Greenberg (Eds.), Selective Hydrocarbon Activation: Principles and Progress, VCH, New York, 1990, p. 467.
[7] P.B. Armentrout, Organometallic bonding and reactivity, in: J.M. Brown, P. Hofmann (Eds.), Topics in Organometallic Chemistry, vol. 4, Springer-Verlag, Berlin, 1999, p. 1.
[8] D.E. Clemmer, L.S. Sunderlin, P.B. Armentrout, J. Phys. Chem. 94 (1990) 3008.
[9] D.E. Clemmer, L.S. Sunderlin, P.B. Armentrout, J. Phys. Chem. 94 (1990) 208.
[10] D.E. Clemmer, P.B. Armentrout, J. Phys. Chem. 95 (1991) 3084.
[11] N. Russo, E. Sicilia, J. Am. Chem. Soc. 123 (2001) 2588.
[12] N. Russo, E. Sicilia, J. Am. Chem. Soc. 124 (2002) 1471.
[13] M. del Carmen Michelini, N. Russo, E. Sicilia, Inorg. Chem. 43 (2004) 4944.
[14] J.L. Elkind, P.B. Armentrout, J. Phys. Chem. 90 (1986) 5736.
[15] R.H. Schultz, J.L. Elkind, P.B. Armentrout, J. Am. Chem. Soc. 110 (1988) 411.
[16] C.L. Haynes, Y.-M. Chen, P.B. Armentrout, J. Phys. Chem. 100 (1996) 111.
[17] D.E. Clemmer, Y.-M. Chen, F.A. Khan, P.B. Armentrout, J. Phys. Chem. 98 (1994) 6522.
[18] D. Schröder, H. Schwarz, D.E. Clemmer, Y.-M. Chen, P.B. Armentrout, V.I. Baranov, D.K. Bohme, Int. J. Mass Spectrom. Ion Process. 161 (1997) 175.
[19] S. Bärsch, I. Kretzschmar, D. Schröder, H. Schwarz, P.B. Armentrout, J. Phys. Chem. A 103 (1999) 5925.
[20] S. Chiodo, O. Kondakova, M. del, C. Michelini, N. Russo, E. Sicilia, A. Irigoras, J.M. Ugalde, J. Phys. Chem. A 108 (2004) 1069.
[21] M. Brönstrup, I. Kretzschmar, D. Schröder, H. Schwarz, Helv. Chim. Acta 81 (1998) 2348.
[22] S.W. Buckner, B.S. Freiser, J. Am. Chem. Soc. 109 (1987) 4715.
[23] S.W. Buckner, J.R. Gord, B.S. Freiser, J. Am. Chem. Soc. 110 (1988) 6606.
[24] D.R.A. Ranatunga, Y.D. Hill, B.S. Freiser, Organometallics 15 (1996) 1242.
[25] K.M. Ervin, P.B. Armentrout, J. Chem. Phys. 83 (1985) 166.
[26] R.H. Schultz, P.B. Armentrout, Int. J. Mass Spectrom. Ion Process. 107 (1991) 29.
[27] L.S. Sunderlin, P.B. Armentrout, J. Phys. Chem. 92 (1988) 1209.
[28] P.A.M. van Koppen, P.R. Kemper, M.T. Bowers, J. Am. Chem. Soc. 114 (1992) 10941.
[29] C.E. Moore, Atomic Energy Levels, vol. III, NSRDS-NBS, 1971, p. 35.
[30] S.K. Loh, L. Lian, D.A. Hales, P.B. Armentrout, J. Chem. Phys. 89 (1988) 3378.
[31] N.F. Dalleska, K. Honma, L.S. Sunderlin, P.B. Armentrout, J. Am. Chem. Soc. 116 (1994) 3519.
[32] N.F. Dalleska, K. Honma, P.B. Armentrout, J. Am. Chem. Soc. 115 (1993) 12125.
[33] F.A. Khan, D.E. Clemmer, R.H. Schultz, P.B. Armentrout, J. Phys. Chem. 97 (1993) 7978.
[34] R.H. Schultz, P.B. Armentrout, J. Chem. Phys. 96 (1992) 1046.
[35] E.R. Fisher, B.L. Kickel, P.B. Armentrout, J. Phys. Chem. 97 (1993) 10204.
[36] D. Gerlich, in: C.-Y. Ng, M. Baer (Eds.), State-selected State-to-state Ion-molecule Reaction Dynamics. Part 1. Experiment, Wiley, New York, 1992, p. 1.
[37] D.A. Hales, L. Lian, P.B. Armentrout, Int. J. Mass Spectrom. Ion Process. 102 (1990) 269.
[38] M.J. Frisch, G.W. Trucks, H.B. Schlegel, et al., Gaussian 98, Revision A.7, Gaussian, Inc., Pittsburgh, PA, 1998.
[39] A.D. Becke, J. Chem. Phys. 98 (1993) 5648.
[40] C. Lee, W. Yang, R.G. Parr, Phys. Rev. B 37 (1988) 785.
[41] P.J. Stephens, F.J. Devlin, C.F. Chabalowski, M.J. Frisch, J. Phys. Chem. 98 (1994) 11623.
[42] J.B. Foresman, Æ. Frisch, Exploring Chemistry with Electronic Structure Methods, 2nd ed., Gaussian, Inc., Pittsburgh, PA, 1996.
[43] A. Irigoras, J.E. Fowler, J.M. Ugalde, J. Am. Chem. Soc. 121 (1999) 8549.
[44] M.T. Rodgers, P.B. Armentrout, J. Chem. Phys. 109 (1998) 1787.
[45] P.B. Armentrout, B.L. Kickel, in: B.S. Freiser (Ed.), Organometallic Ion Chemistry, Kluwer Academic Publishers, Dordrecht, 1996, p. 1.
[46] P.B. Armentrout, J. Simons, J. Am. Chem. Soc. 114 (1992) 8627.
[47] M.R. Sievers, Y.-M. Chen, P.B. Armentrout, J. Chem. Phys. 105 (1996) 6322.
[48] X.-G. Zhang, P.B. Armentrout, J. Phys. Chem. A 107 (2003) 8915.
[49] G. Gioumousis, D.P. Stevenson, J. Chem. Phys. 29 (1958) 294.
[50] J.L. Elkind, P.B. Armentrout, J. Phys. Chem. 90 (1986) 5736.
[51] J.B. Schilling, W.A. Goddard III, J.L. Beauchamp, J. Phys. Chem. 91 (1987) 5616.
[52] L.G.M. Pettersson, C.W. Bauschlicher Jr., S.R. Langhoff, H. Partridge, J. Chem. Phys. 87 (1987) 481.
[53] M.W. Chase, C.A. Davies, J.R. Downey, D.J. Frurip, R.A. McDonald, A.N. Syverud, J. Phys. Chem. Ref. Data 14 (Suppl. 1) (1988) (JANAF Tables).
[54] E.R. Fisher, J.L. Elkind, D.E. Clemmer, R. Georgiadis, S.K. Loh, N. Aristov, L.S. Sunderlin, P.B. Armentrout, J. Chem. Phys. 93 (1990) 2676.
[55] 298 K Heat of formation of CH_3NH_2 taken from J.B. Pedley, R.D. Naylor, S.P. Kirby, Thermochemical Data of Organic Compounds, 2nd ed., Chapman & Hall, New York, 1986, and corrected to 0 K using vibrational frequencies from T. Shimanouchi, Tables of Molecular Vibrational Frequencies Consolidated, vol. I, NSRDS-NBS 39 (1972) 1 ;
0 K Heat of formation for CH_3 taken from J. Berkowitz, G.B. Ellison, D. Gutman, J. Phys. Chem. 98 (1994) 2744;
0 K Heat of formation for NH and NH_2 taken from W.R. Anderson, J. Phys. Chem. 93 (1989) 530.
[56] S.R. Langhoff, C.W. Bauschlicher Jr., H. Partridge, M. Sodupe, J. Phys. Chem. 95 (1991) 10677.
[57] D. Walter, P.B. Armentrout, J. Am. Chem. Soc. 120 (1998) 3176.
[58] L.S. Sunderlin, P.B. Armentrout, J. Phys. Chem. 92 (1988) 1209.
[59] N. Aristov, P.B. Armentrout, J. Phys. Chem. 91 (1987) 6178.
[60] C. Rue, P.B. Armentrout, I. Kretzschmar, D. Schröder, J.N. Harvey, H. Schwarz, J. Chem. Phys. 110 (1999) 7858.
[61] D.G. Musaev, K. Morokuma, N. Koga, K.A. Nguyen, M.S. Gordon, T.R. Cundari, J. Phys. Chem. 97 (1993) 11435.
[62] M. Brönstrup, D. Schröder, H. Schwarz, Chem. Eur. J. 5 (1999) 1176.
[63] D. Schröder, H. Schwarz, Int. J. Mass Spectrom. 227 (2003) 121.
[64] T.F. Magnera, D.E. David, J. Michl, J. Am. Chem. Soc. 111 (1989) 4100.
[65] C.J. Cassady, B.S. Freiser, J. Am. Chem. Soc. 106 (1984) 6176.
[66] E. Murad, J. Chem. Phys. 73 (1980) 1381.
[67] L.N. Gorokhov, M.I. Milushin, A.M. Emelyanov, High Temp. Sci. 26 (1990) 395.